

# Recent advances in two-dimensional photovoltaic devices

**Haoyun Wang<sup>1,‡</sup>, Xingyu Song<sup>1,‡</sup>, Zexin Li<sup>1</sup>, Dongyan Li<sup>1</sup>, Xiang Xu<sup>1</sup>, Yunxin Chen<sup>1</sup>, Pengbin Liu<sup>1</sup>, Xing Zhou<sup>1,†</sup>, and Tianyou Zhai<sup>1,2,3,†</sup>**

<sup>1</sup>State Key Laboratory of Materials Processing and Die & Mould Technology, School of Materials Science and Engineering, Huazhong University of Science and Technology, Wuhan 430074, China

<sup>2</sup>Research Institute of Huazhong University of Science and Technology in Shenzhen, Shenzhen 518057, China

<sup>3</sup>Optics Valley Laboratory, Wuhan 430074, China

**Abstract:** Two-dimensional (2D) materials have attracted tremendous interest in view of the outstanding optoelectronic properties, showing new possibilities for future photovoltaic devices toward high performance, high specific power and flexibility. In recent years, substantial works have focused on 2D photovoltaic devices, and great progress has been achieved. Here, we present the review of recent advances in 2D photovoltaic devices, focusing on 2D-material-based Schottky junctions, homojunctions, 2D–2D heterojunctions, 2D–3D heterojunctions, and bulk photovoltaic effect devices. Furthermore, advanced strategies for improving the photovoltaic performances are demonstrated in detail. Finally, conclusions and outlooks are delivered, providing a guideline for the further development of 2D photovoltaic devices.

**Key words:** two-dimensional materials; photovoltaic devices; photodetectors; solar cells; heterostructures

**Citation:** H Y Wang, X Y Song, Z X Li, D Y Li, X Xu, Y X Chen, P B Liu, X Zhou, and T Y Zhai, Recent advances in two-dimensional photovoltaic devices[J]. *J. Semicond.*, 2024, 45(5), 051701. <https://doi.org/10.1088/1674-4926/45/5/051701>

## 1. Introduction

Photovoltaic devices play an important part in solar-energy conversion, image sensing, communication, and other extensive fields<sup>[1–9]</sup>. Although photovoltaic devices based on conventional bulk semiconductors have been widely applied, the limitations such as low absorption coefficient, lattice mismatch, brittleness and surface dangling bonds impede the further development in high-performance and wearable photovoltaic devices.

In recent years, two-dimensional (2D) materials have attracted increasing interest due to the unique optoelectronic properties, including dangling-bond-free surface<sup>[10–16]</sup>, strong light–matter interaction<sup>[17–28]</sup>, broadband absorption<sup>[29–41]</sup> and flexibility<sup>[42–48]</sup>. Compared with conventional semiconductors, 2D materials exhibit great advantages in photovoltaic devices. Table 1 shows the properties of 2D materials and its significance for photovoltaic devices. Firstly, the dangling-bond-free surface allows different 2D materials to be integrated by van der Waals (vdW) force without the lattice mismatch. Therefore, the carrier transportation can be modulated by band engineering, and broadband light absorption can be achieved by stacking 2D materials with different bandgaps<sup>[49–54]</sup>. Moreover, such dangling-bond-free surface is self-passivated, avoiding the complex surface passivation process<sup>[55–57]</sup>. Secondly, the ultrathin body of 2D materials enables efficient modulation of electrical properties by exter-

nal field and chemical surroundings, thus the photoelectric performances can be effectively modulated, providing new pathways for improving the photovoltaic performances<sup>[58–64]</sup>. Thirdly, 2D materials such as transition metal dichalcogenides (TMDs) exhibit strong light–matter interaction, showing larger light absorption in comparison with bulk semiconductors in nanoscale thickness, and thus ultra-thin photovoltaic devices can be achieved through 2D materials<sup>[65–67]</sup>. Last but not least, the mechanical flexibility of 2D materials makes them applicable in flexible and wearable photovoltaic devices. Therefore, 2D materials provide great opportunities for next-generation photovoltaic devices. In recent years, substantial progress of 2D photovoltaic devices has been made. A comprehensive summary and prediction for the further development of 2D photovoltaic devices are in urgent need.

Here, we demonstrate the recent advances in 2D photovoltaic devices. We first present the general classification of 2D photovoltaic devices, including 2D-material-based Schottky junctions, homojunctions, 2D–2D heterojunctions, 2D–3D heterojunctions, and bulk photovoltaic effect (BPVE) devices. Subsequently, recent representative researches on each structure are presented, and the strategies for improving the photovoltaic performances are demonstrated in detail. Finally, conclusions and outlooks are delivered, providing a guideline for the further development of 2D photovoltaic devices.

## 2. 2D photovoltaic devices

General photovoltaic device requires a built-in electric field, where the photo-generated carriers are separated and the photocurrent is generated. The built-in field can be generated by fabricating heterojunctions, homojunctions and Schottky junctions. The self-passivated surface of 2D materials provide a platform for fabricating devices through vdW interaction, and the ultrathin nature makes it highly tunable by exter-

H Y Wang and X Y Song contributed equally to this work and should be considered as co-first authors.

Correspondence to: X Zhou, [zhoux0903@hust.edu.cn](mailto:zhoux0903@hust.edu.cn); T Y Zhai, [zhaity@hust.edu.cn](mailto:zhaity@hust.edu.cn)

Received 19 DECEMBER 2023; Revised 23 JANUARY 2024.

©2024 Chinese Institute of Electronics

Table 1. The properties of 2D materials and its significance for photovoltaic devices.

Properties of 2D materials	Significance for photovoltaic devices
Dangling-bond-free surface	Van der Waals integration for band engineering self-passivated surface
Ultrathin body	Strong modulation of electrical properties
Strong light–matter interaction	Ultra-thin devices with high performances
Mechanical flexibility	Flexible devices

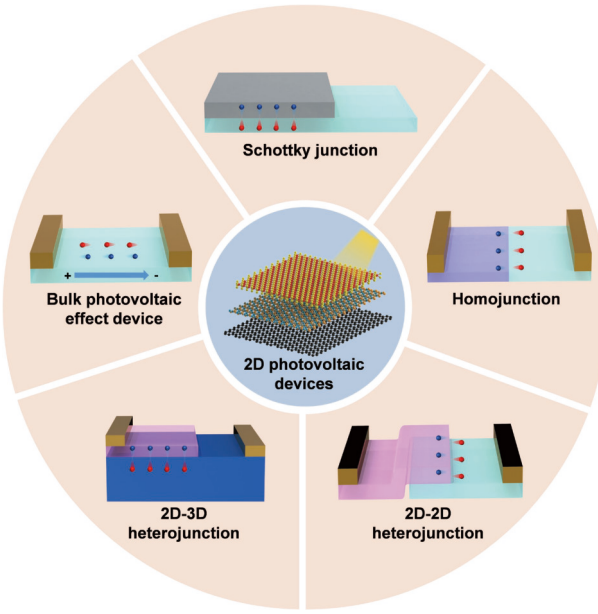


Fig. 1. (Color online) The general classification of 2D photovoltaic devices, including Schottky junctions, homojunctions, 2D–2D heterojunctions, 2D–3D heterojunctions, and BPVE devices. The blue spheres represent holes and the red spheres represent electrons.

nal fields and chemical surroundings. Moreover, novel properties such as BPVE have been discovered in 2D materials. Thus, 2D materials provide great opportunity for novel photovoltaic devices. Fig. 1 shows the classification of 2D photovoltaic devices, including Schottky junctions, homojunctions, 2D–2D heterojunctions, 2D–3D heterojunctions, and BPVE devices.

## 2.1. 2D Schottky junction devices

Schottky junctions are widely used in photovoltaic devices. Due to the difference in work functions between metal and semiconductors, charge transfer occurs when metal and semiconductor contact, and thus a built-in field is generated at the interface of the semiconductor, which separates photo-generated electron–hole pairs under illumination, resulting in photovoltaic effect.

Schottky junction photovoltaic devices based on 2D materials have been widely researched<sup>[68–72]</sup>. However, the ultrathin body makes 2D materials highly sensitive to the contact quality<sup>[73–76]</sup>. Conventional evaporation method to make metal–semiconductor contact usually introduces interface defects due to the impact of high-energy metal atoms, leading to severe Fermi-level pinning effect and unpredictable Schottky barrier. Moreover, the interface defects act as recombination center, reducing the carrier collection efficiency<sup>[77–81]</sup>. These factors become the limits of high-performance 2D Schottky photovoltaic devices.

In recent years, vdW metal contact method has been developed. Due to the self-passivated surface of 2D materials,

vdW metal contact can be realized by transferring metal to the 2D materials. In 2018, Liu *et al.* reported the creation of vdW metal–semiconductor junction, as shown in Fig. 2(a)<sup>[82]</sup>. Compared with conventional evaporation method, the non-destructive method creates an interface that is free from lattice destruction and defects, eliminating the Fermi-level pinning effect. As a result, the value of Schottky barrier approaches the Schottky–Mott limit, indicating an ideal contact. Thus, Schottky junction can be designed by selecting metals and semiconductors with large difference in work functions. The authors demonstrated an Ag/MoS<sub>2</sub>/Pt asymmetric-contact Schottky device (Fig. 2(b)), and an excellent ideality factor of 1.09 is obtained, indicating an ideal Schottky diode. A pronounced photovoltaic effect under illumination is observed, as shown in Fig. 2(c), with the open-circuit voltage ( $V_{OC}$ ) reaching 1.02 V in one-layer device and 0.76 V in seven-layer device. In 2021, Zhang *et al.* reported a MoS<sub>2</sub>/1T'-MoTe<sub>2</sub> vdW Schottky junction, and also showed that the vdW integration of the 2D semiconductor and 2D metal can effectively inhibit the Fermi-level pinning effect caused by lattice destruction and defects, resulting in ideal Schottky barrier height<sup>[83]</sup>. Furthermore, this work introduced the acid-induced sulfur vacancy self-healing (SVSH) effect to reduce the sulfur vacancies in the MoS<sub>2</sub>, which significantly decreases the intrinsic doping level of MoS<sub>2</sub>. As a result, the Schottky barrier width is evidently enlarged. The ideal Schottky junction exhibits a good ideality factor of ~1.6, and improved photovoltaic performances with high external quantum efficiency (EQE) of 20%.

To achieve high efficiency of carrier collection and realize scalable photoactive area, vertical contact device shows more advantages in photovoltaic devices. In 2019, Went *et al.* developed a transfer process for fabricating Schottky junction photovoltaic device with vertical vdW contact, as shown in Fig. 2(d)<sup>[84]</sup>. WS<sub>2</sub> is used as absorber layer, and Au and Ag electrodes are used as asymmetric contacts. Due to the high-quality vdW interface and high carrier collection efficiency in the vertical channel, the device exhibits high photovoltaic performances. As shown in Fig. 2(e), high photovoltaic performances with  $V_{OC}$  of 256 mV, short circuit current ( $I_{SC}$ ) of 4.10 mA/cm<sup>2</sup>, EQE of ~40%, and power conversion efficiency (PCE) of 0.46% are achieved, while similar device made with evaporated metal contact shows negligible photovoltaic effect. Moreover, the developed direct transfer process eliminates the lithography process, providing a feasible way for batch fabrication.

However, the EQE of most reported 2D photovoltaic devices are below 50%, which is much lower than the theoretical limit<sup>[85]</sup>. The main challenge lies in the photo-generated carrier recombination loss in channel. In 2022, Wang *et al.* demonstrated a 2D photovoltaic device with minimized defects and carrier recombination in channel, as shown in Fig. 2(f)<sup>[86]</sup>. Graphene/WS<sub>2</sub>/Pt vertical Schottky device is fabricated, and the vdW metal contact is applied to realize an interface with-

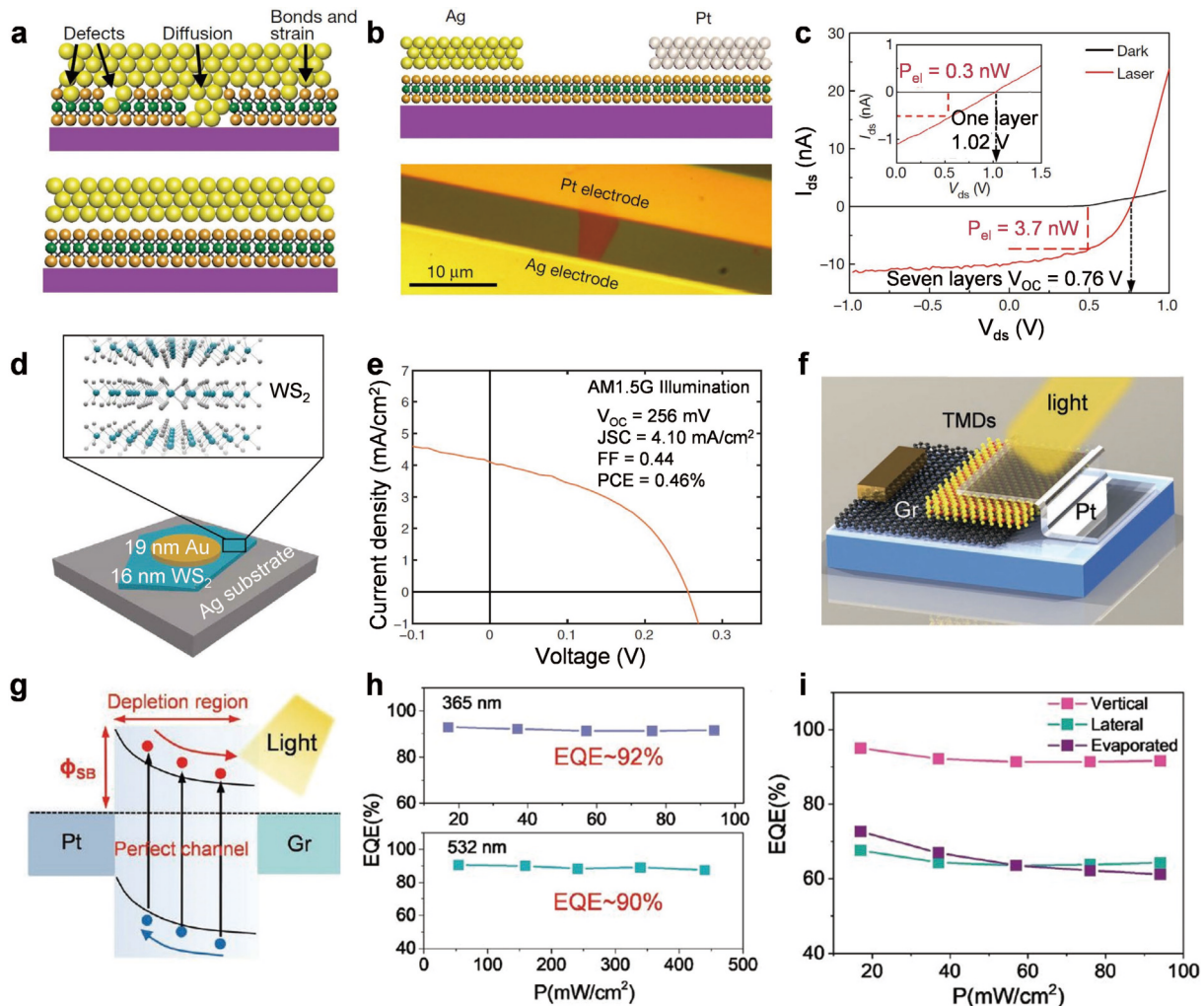


Fig. 2. (Color online) (a) Schematic of the conventional evaporated metal contact interface and vdW metal contact interface. (b) Schematic and optical image of Ag/MoS<sub>2</sub>/Pt asymmetric contact Schottky device. (c) The  $I$ - $V$  characteristic of the Ag/MoS<sub>2</sub>/Pt device in dark and 532-nm laser. (a–c) Reproduced with permission<sup>[82]</sup>. Copyright 2018, Springer Nature. (d) Schematic of the Au/WS<sub>2</sub>/Ag vertical vdW contact Schottky device. (e) The  $I$ - $V$  characteristic of the device under AM 1.5G illumination. (d, e) Reproduced with permission<sup>[84]</sup>. Copyright 2019, American Association for the Advancement of Science. (f) Schematic of the graphene/WS<sub>2</sub>/Pt vertical vdW contact Schottky device. (g) The band diagram under illumination of the graphene/WS<sub>2</sub>/Pt device. (h) The EQE of the graphene/WS<sub>2</sub>/Pt device under 365-nm and 532-nm laser with varied power density. (i) The EQE comparison of the vertical vdW contact device, lateral device and evaporated contact devices. (f–i) Reproduced with permission<sup>[86]</sup>. Copyright 2022, Wiley-VCH.

out defects and Fermi-level pinning. Thereby, a large Schottky barrier can be realized by adopting metal with large work functions such as Pt. Furthermore, by modulating the thickness of WS<sub>2</sub>, the trade-off between carrier collection efficiency and light absorption is addressed. As a result, under illumination, the carriers can be swiftly separated in the depleted channel and collected by electrodes without recombination loss. As shown in Fig. 2(g), efficient carrier transportation without loss is realized. As shown in Figs. 2(h) and 2(i), a high EQE of 92% is achieved, which approaches the theoretical limit. Moreover, the proposed strategy of fabricating high-performance photovoltaic devices can be extended to other 2D materials such as MoSe<sub>2</sub> and WSe<sub>2</sub>.

Electron-selective contact has also been demonstrated effective to improve the photovoltaic performances. In 2022, Kim *et al.* reported a Pt/WSe<sub>2</sub>/WO<sub>x</sub>/Gr photovoltaic device<sup>[87]</sup>. A WO<sub>x</sub> layer is introduced by plasma treatment of the WSe<sub>2</sub> surface and acts as electron-selective contact, which promotes the extraction of electrons and inhibits the extraction

of holes to graphene, reducing the recombination loss at the contact interfaces. As a result, a PCE up to 5.44% is realized. Furthermore, Nazif *et al.* demonstrated a high-specific-power flexible solar cell based on 2D Schottky device<sup>[88]</sup>. Vertical Au/WSe<sub>2</sub>/Gr vdW contact Schottky junction is fabricated on flexible and lightweight polyimide substrate. MoO<sub>x</sub> capping is used for doping as well as anti-reflection. High PCE of 5.1% under AM 1.5G is achieved. Meanwhile, the bending test suggests consistent performance levels under bending, and the use of ultrathin polyimide substrate achieves a high specific power of 4.4 W·g<sup>-1</sup>.

## 2.2. 2D homojunction devices

P–n junction is another building block of photovoltaics. When a p–n junction is fabricated, the holes transfer from p-type material to n-type material, and electrons transfer from n-type material to p-type material, thus forming a built-in field at the junction interface, which separates photo-generated electron–hole pairs under illumination, resulting in photovoltaic effect. P–n homojunctions have been widely used in

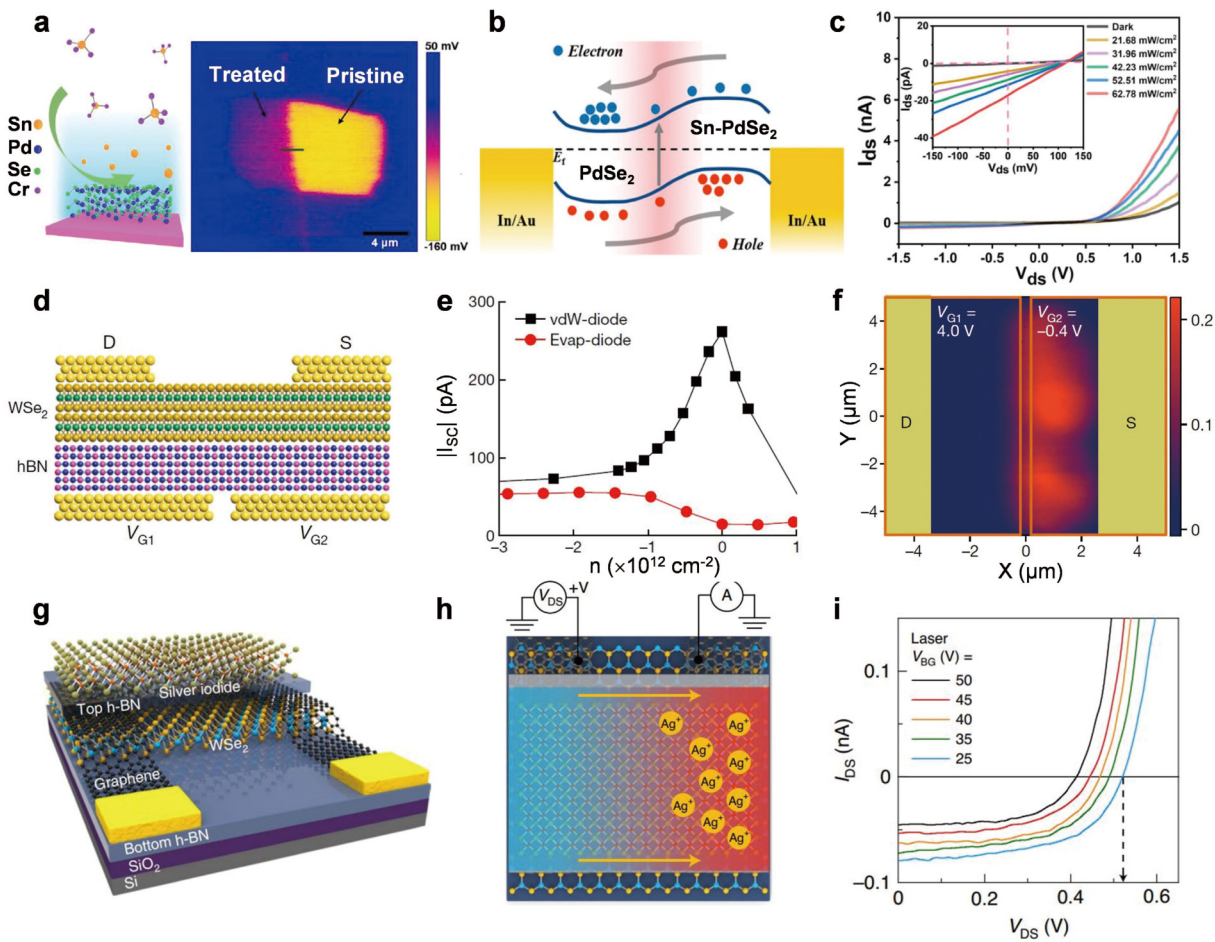


Fig. 3. (Color online) (a) Schematic illustration of ion exchanging process (left), and the KPFM image of the doped PdSe<sub>2</sub> in-plane homojunction (right). (b) The band diagram of the doped PdSe<sub>2</sub> homojunction. (c)  $I-V$  curves of the PdSe<sub>2</sub> homojunction under 532-nm laser with varied power density. (a–c) Reproduced with permission<sup>[100]</sup>. Copyright 2022, American Chemical Society. (d) Schematic of the split-gate WSe<sub>2</sub> device. (e) The  $I_{SC}$  versus carrier density of vdW contact device and evaporated device. (f) The photocurrent mapping characterization under zero bias. (d–f) Reproduced with permission<sup>[106]</sup>. Copyright 2021, Springer Nature. (g) Schematic of the WSe<sub>2</sub> device with a silver iodide doping layer. (h) Illustration of the Ag<sup>+</sup> ion doping mechanism of the device. (i)  $I-V$  curves of the homojunction under 532-nm laser illumination. (g–i) Reproduced with permission<sup>[58]</sup>. Copyright 2020, Springer Nature.

photovoltaic devices. Extensive researches have been focused on the p–n homojunctions based on 2D materials, and multiple strategies for realizing 2D homojunctions have been developed, such as doping and external field modulation<sup>[89–97]</sup>.

Conventional doping method for bulk semiconductors could introduce severe defect states in ultrathin 2D materials, which seriously degrade the performances<sup>[98, 99]</sup>. Hence, it is vital to develop novel doping methods for 2D photovoltaic devices. In 2022, Li *et al.* developed a universal p-type doping method for TMDs<sup>[100]</sup>. As shown in Fig. 3(a), the SnCl<sub>4</sub> solution is used to treat the 2D materials, where the Sn<sup>4+</sup> ion exchanging process can effectively reduce the electron concentration in TMDs, and the Kelvin probe force microscopy (KPFM) image shows an evident increase in the work function of doped PdSe<sub>2</sub>. Moreover, by changing the concentration of SnCl<sub>4</sub> solution, the doping level can be effectively modulated. By this means, an in-plane homojunction is fabricated (Fig. 3(b)), and pronounced photovoltaic effect is observed (Fig. 3(c)). 2D p–n homojunction photovoltaic devices based on other doping methods have also been reported, such as aluminum-doped black phosphorus (BP) homojunction<sup>[101]</sup>, boron-doped BP homojunction<sup>[102]</sup>, WSe<sub>2</sub>

homojunction metal contact doping<sup>[103]</sup>, etc. P–i–n homojunctions can also be realized by doping of 2D materials. The introduction of intrinsic region extends the depletion region, where the carriers can be efficiently separated without recombination, thus higher carrier collection efficiency can be realized. In 2021, Zhang *et al.* fabricated a WSe<sub>2</sub> p–i–n diode by surface plasma treatment doping<sup>[104]</sup>. O<sub>2</sub> plasma and Ar plasma are used to treat the contact region and obtain p-type and n-type doping. The photoactive volume is increased by adding an intrinsic layer to extend the depletion region, which can effectively separate photo-generated carriers, resulting in enhanced photovoltaic performances, including  $I_{SC}$  of 0.57 μA and  $V_{OC}$  of 0.34 V. Lee *et al.* reported a MoTe<sub>2</sub> p–i–n homojunction realized by selective H-doping and split-gate modulation<sup>[105]</sup>. The  $I_{SC}$  of the p–i–n junction is 70 pA, showing large improvement compared with 15 pA of the p–n junction. The improvement is attributed to the greater depletion region with higher efficiency of carrier separation.

However, the chemical doping methods for fabricating p–n homojunction still introduce impurity dopants, which could degrade the electrical performances of 2D materials, and the doping is irreversible. In recent years, external field modulation has been developed for fabricating 2D p–n homo-

junctions. In 2021, Chen *et al.* fabricated split-gate WSe<sub>2</sub> devices (Fig. 3(d)) to modulate the electron and hole doping in WSe<sub>2</sub>, and investigated the exciton behavior under illumination<sup>[106]</sup>. VdW metal contact is used to obtain an interface with minimum Shockley–Read–Hall recombination, and thus the intrinsic photophysics of the device can be realized. A p–n homojunction is obtained by electrostatic field modulation in the split-gate geometry. Under illumination, photovoltaic effect is observed, and the  $I_{SC}$  under the modulation of gate voltage is investigated. In vdW contact device, a peak of  $I_{SC}$  appears at low charge density by the gate modulation (Fig. 3(e)). The peak  $I_{SC}$  is attributed to the suppressed exciton–charge Auger recombination at low charge density. However, in evaporated contact device, the peak  $I_{SC}$  disappears due to the influence of interface defects. The photocurrent mapping shows much longer exciton diffusion length at low charge density region (Fig. 3(f)), further confirming the suppressed exciton–charge Auger recombination. The photovoltaic performances are greatly enhanced due to the reduced carrier recombination, EQE of 83.6% and  $V_{OC}$  of 0.75 V are achieved in a three-layer device. In addition, ferroelectric materials have also been utilized for modulating 2D materials due to the strong electrostatic field and nonvolatile characteristic. In 2020, Wu *et al.* demonstrated ferroelectric polarization enabled MoTe<sub>2</sub> p–n junctions<sup>[107]</sup>. Ferroelectric P(VDF–TrFE) is applied as dielectric and split-gate electrodes are used to modulate the channel. The device can be reconfigured as n–n, p–p, p–n, and n–p junctions by changing the polarization directions. High rectification ratio of  $5 \times 10^5$  is realized in the p–n junction, and high photovoltaic performances including EQE of 40% and PCE of 2.5% are achieved.

Novel doping strategies have been explored in recent years. In 2020, Lee *et al.* reported a reversible solid-state doping of 2D materials by introducing superionic silver iodide layer in WSe<sub>2</sub> device, as shown in Fig. 3(g)<sup>[58]</sup>. By applying an electric field to the device at a temperature above the superionic phase transition temperature, the Ag<sup>+</sup> can be selectively accumulated or depleted at doping locations, thus nonvolatile p-type or n-type doping can be reversibly realized in WSe<sub>2</sub> channel, as shown in Fig. 3(h). The p–n homojunction exhibits pronounced photovoltaic effect with a high  $V_{OC}$  of ~0.52 V (Fig. 3(i)). In addition, p–n homojunctions can also be realized by the intrinsic ion migration in 2D materials. In 2023, Zhu *et al.* presented a p–n homojunction based on 2D CulnP<sub>2</sub>S<sub>6</sub><sup>[108]</sup>. The Cu<sup>+</sup> ions migrate under the in-plane electric field, leading to p-type and n-type doped area, forming a lateral p–n homojunction. The p–n junction exhibits distinct rectification and photovoltaic performances. Moreover, the rectification and photovoltaic behavior can be effectively tuned and reversed by changing the poling voltage. As a result, good photovoltaic performances including  $V_{OC}$  of 0.3 V and  $J_{SC}$  of 20 mA/cm<sup>2</sup> are achieved.

### 2.3. 2D–2D p–n heterojunction devices

Owing to the self-passivated surface, different 2D materials can be assembled through vdW interaction despite lattice mismatch, thus p–n heterojunctions can be easily fabricated. VdW integration allows band engineering for charge transfer modulation and complementary bandgaps. Therefore, 2D p–n heterojunctions provide great potential for high-performance photovoltaic devices. 2D p–n heterojunc-

tion have been widely studied in recent years<sup>[109–115]</sup>.

In 2021, Zou *et al.* reported a GaSe/MoS<sub>2</sub> p–n heterojunction. Due to the high-quality heterojunction interface and the type-II band alignment, a large  $V_{OC}$  of 0.61 V is achieved<sup>[116]</sup>. Furthermore, heterojunctions provide the advantage of combining the characteristic of different materials. For example, Zhao *et al.* demonstrated a BP/InSe heterojunction in 2018, in which the BP provides broadband light absorption and polarization sensitivity, and the InSe provides high electron mobility. As a result, a broadband, polarization-sensitive, and fast response photovoltaic device is obtained<sup>[117]</sup>. Broadband photovoltaic devices have been realized by involving narrow-bandgap materials in p–n heterojunctions, such as WSe<sub>2</sub>/Bi<sub>2</sub>Te<sub>3</sub><sup>[118]</sup>, b-As<sub>0.4</sub>P<sub>0.6</sub>/MoTe<sub>2</sub><sup>[119]</sup>, AsP/InSe<sup>[120]</sup>, etc.

Various 2D p–n heterojunction photovoltaic devices have been explored. However, the EQE of most reported devices are below 55%. One of the main challenges is the interface carrier recombination. In 2019, Wu *et al.* proposed a MoS<sub>2</sub>/AsP p–n junction, using AsP as a carrier selective contact and forming a unilaterally depleted type-I heterojunction, as shown in Fig. 4(a)<sup>[121]</sup>. A large depletion region is formed in the MoS<sub>2</sub> due to the large difference in work functions between MoS<sub>2</sub> and AsP. Under illumination, photo-generated carriers in MoS<sub>2</sub> are effectively separated by the built-in field, and only photo-generated electrons can transfer through the interface and are collected by the AsP via the rapid recombination with the opposite carriers in the accumulation region. Meanwhile, the holes in MoS<sub>2</sub> side transfer to the source electrode (Fig. 4(b)). Thus, the interface recombination of the carriers can be effectively suppressed, significantly enhancing the carrier collection efficiency. As a result, the device exhibits high photovoltaic performances with an  $I_{SC}$  of 1.3 μA, a  $V_{OC}$  up to 0.61 V (Fig. 4(c)) and a high EQE of 71%. Furthermore, the unilaterally depleted heterojunction is applicable to other 2D materials, such as MoS<sub>2</sub>/BP heterojunction.

The photovoltaic performances of p–n heterojunctions are limited by the built-in field, impeding the further development. On this issue, Jin *et al.* demonstrated a 2D CsPbBr<sub>3</sub>/CdS p–n junction with excellent excitonic photovoltaic effect to address the limitation of built-in field in 2020 (Fig. 4(d))<sup>[122]</sup>. 2D CsPbBr<sub>3</sub> possess large exciton binding energy, and the photo-generated excitons diffuse to the interface and dissociate under illumination. As a result, a large chemical potential energy gradient is formed to enhance the carrier separation (Fig. 4(e)). The photo-generated carriers are effectively separated under effect of both built-in field and the chemical potential energy, leading to improved carrier separation efficiency and subsequently the photovoltaic performance. As shown in Fig. 4(f), large  $V_{OC}$  of ~0.76 V and PCE of ~17.5% are achieved.

The low light absorption efficiency is another challenge for 2D p–n heterojunction photovoltaic devices. Decorating 2D p–n heterojunctions using materials with large light absorption is an effective strategy to improve the light absorption. In 2022, Zeng *et al.* demonstrated a WSe<sub>2</sub>/MoS<sub>2</sub> p–n junction decorated by PbS quantum dots (QDs) (Fig. 4(g))<sup>[123]</sup>. The PbS QDs act as the light-sensitive layer, and the electrons produced in the QDs layer can be effectively collected by the MoS<sub>2</sub> under the built-in field. Then, the light absorption is significantly enhanced. As shown in Fig. 4(h), the

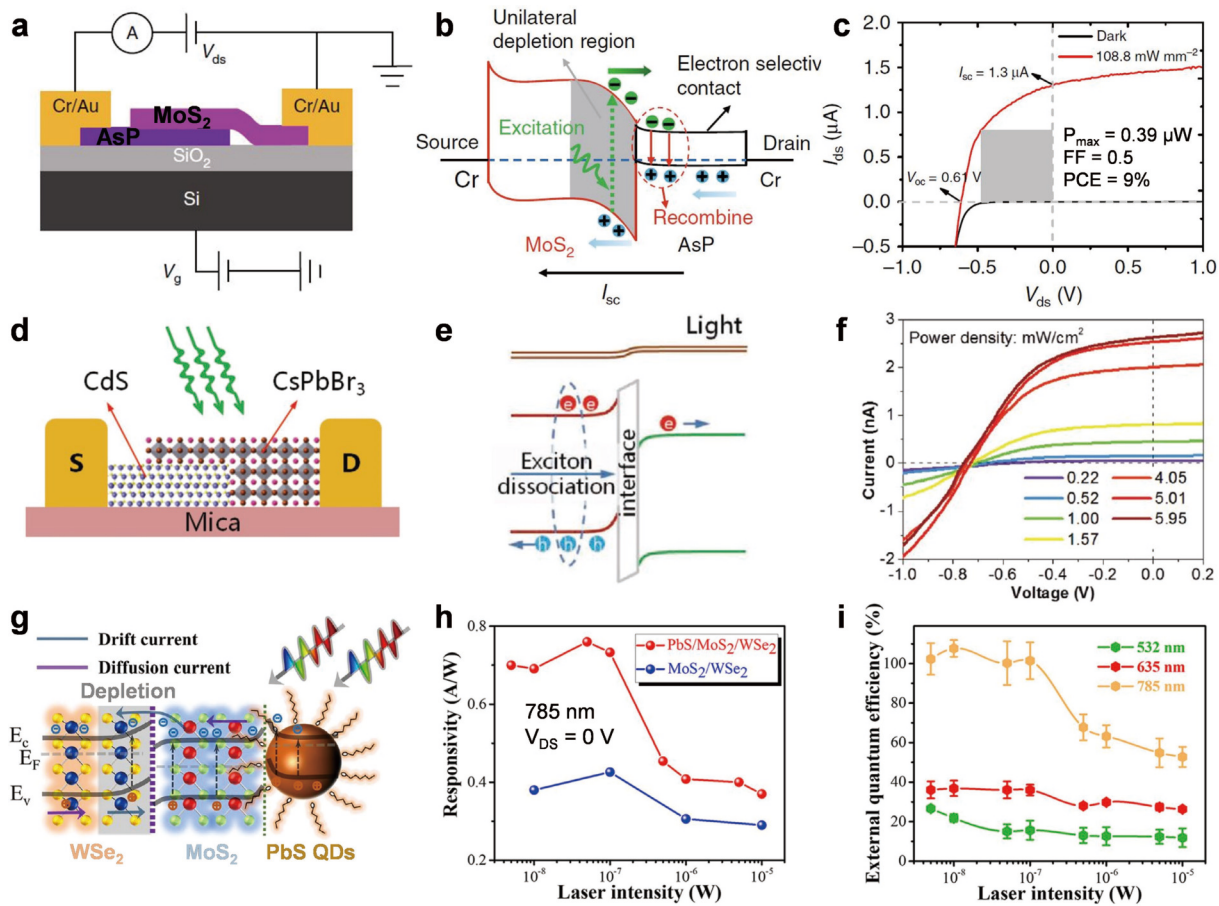


Fig. 4. (Color online) (a) Schematic of the unilaterally depleted  $\text{MoS}_2/\text{AsP}$  heterojunction device. (b) The band diagram of the heterojunction device. (c) The  $I-V$  characteristics of the  $\text{MoS}_2/\text{AsP}$  junction in dark and under 532-nm laser. (a–c) Reproduced with permission<sup>[121]</sup>. Copyright 2019, Springer Nature. (d) Schematic of the  $\text{CsPbBr}_3/\text{CdS}$  p–n junction device. (e) The band diagram of the  $\text{CsPbBr}_3/\text{CdS}$  p–n heterojunction. (f)  $I-V$  curves of the  $\text{CsPbBr}_3/\text{CdS}$  device under 500-nm laser with variable power density. (d–f) Reproduced with permission<sup>[122]</sup>. Copyright 2020, Wiley-VCH. (g) The band diagram of the PbS QDs decorated  $\text{WSe}_2/\text{MoS}_2$  p–n junction. (h) Photoresponsivity of the device  $\text{WSe}_2/\text{MoS}_2$  heterojunction with and without PbS QDs. (i) EQE of the PbS QDs decorated  $\text{WSe}_2/\text{MoS}_2$  device under incident light of varied wavelength. (g–i) Reproduced with permission<sup>[123]</sup>. Copyright 2022, American Chemical Society.

device with PbS QDs layer exhibits greatly enhanced photoresponse and achieves a maximum EQE of 100% (Fig. 4(i)). 2D perovskites with strong light absorption also provide great potential for overcoming the challenge of low-absorption efficiency<sup>[124–126]</sup>. Fang *et al.* reported a  $\text{Cs}_2\text{AgBiBr}_6/\text{WS}_2$  p–n heterojunction<sup>[127]</sup>. The 2D perovskite  $\text{Cs}_2\text{AgBiBr}_6$  serves as a light-sensitive layer, which enhances the sensitivity of the  $\text{WS}_2$ , and prominent charge transfer at the junction interface is observed. Moreover, a vertical-stacked graphene layer is used to further enhance the carrier collection efficiency. As a result, pronounced photovoltaic effect with a large  $V_{OC}$  of ~0.75 V is achieved. Wang *et al.* reported a perovskite  $\text{BP}/\text{MoS}_2$  heterojunction<sup>[128]</sup>. The  $\text{MAPbI}_3$  is used as a light-sensitive layer to improve the performance of  $\text{BP}/\text{MoS}_2$  p–n junction, and the photo-generated carriers in  $\text{MAPbI}_3$  can be effectively transferred to the BP layer. As a result, a high EQE of ~80% is achieved.

Contact engineering has also been proved as an effective method to boost the performances of 2D p–n heterojunctions. In 2020, Yang *et al.* reported a  $\text{WSe}_2/\text{MoS}_2$  p–n heterojunction with atomically thin  $\text{WO}_x$  on the surface of  $\text{WSe}_2$ , which serves as a charge transport layer<sup>[129]</sup>. A strong built-in electric field is formed at the  $\text{WSe}_2/\text{WO}_x$  junction, promoting the extraction of holes to graphene while blocking the trans-

port of the dissociated electrons. In this manner, the rapid recombination of the separated charges at heterojunction is inhibited, resulting in significantly enhanced photovoltaic performance. The PCE increases from 0.7% to 5.0% after adding the  $\text{WO}_x$  layer.

The carrier collection efficiency is also a key factor in photovoltaic performances. In a p–n junction, a depletion region is generated at the interface of heterojunction. The photo-generated carriers can be swiftly separated and swept out of the depletion region by the built-in field without recombination. However, during the diffusion process in the undepleted channel, carrier recombination occurs, resulting in decreased carrier collection efficiency and limited EQE<sup>[105, 130]</sup>. Therefore, the carrier transportation in the undepleted channel should be minimized. Fabricating vertical-channel p–n junctions with ultrathin 2D materials can minimize the carrier diffusion in the undepleted channel, meanwhile, large photoactive area can be obtained. In 2017, Wong *et al.* reported a  $\text{WSe}_2/\text{MoS}_2$  p–n heterojunction with graphene and Au as top and bottom electrodes, as shown in Fig. 5(a)<sup>[85]</sup>. The quantum efficiency of device with graphene top electrode shows great improvement compared with that of the device without graphene top electrode (Fig. 5(b)), confirming the significant improvement of carrier collection efficiency in the verti-

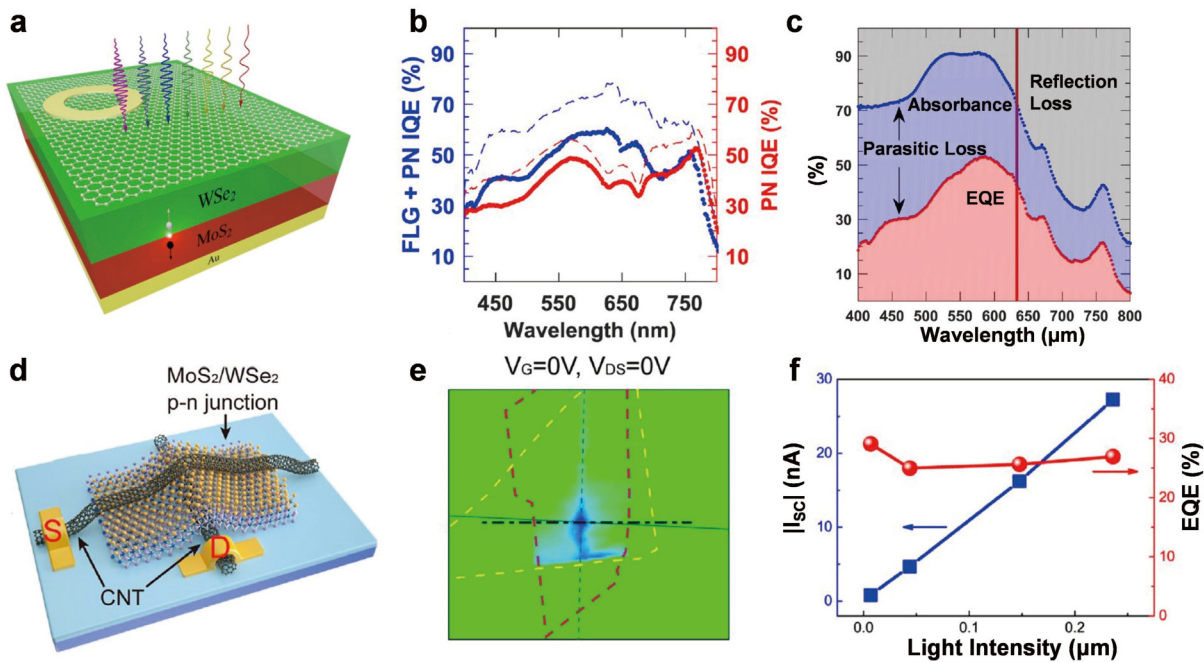


Fig. 5. (Color online) (a) Schematic of the vertical WSe<sub>2</sub>/MoS<sub>2</sub> heterojunction. (b) The quantum efficiency of the p–n junction with and without graphene top electrode. (c) The EQE and absorbance of the vertical WSe<sub>2</sub>/MoS<sub>2</sub> p–n heterojunction. (a–c) Reproduced with permission<sup>[85]</sup>. Copyright 2017, American Chemical Society. (d) Schematic of the CNT/WSe<sub>2</sub>/MoS<sub>2</sub>/CNT vertical point p–n heterojunction. (e) The photocurrent mapping image of the device at zero bias. (f)  $I_{SC}$  and EQE of the device under 520-nm laser illumination with varied power density. (d–f) Reproduced with permission<sup>[131]</sup>. Copyright 2020, American Chemical Society.

cal channel device. As a result, high EQE up to 50% is achieved (Fig. 5(c)). In 2020, Zhang *et al.* reported carbon nanotube (CNT)/WSe<sub>2</sub>/MoS<sub>2</sub>/CNT vertical point p–n heterojunctions, as shown in Fig. 5(d)<sup>[131]</sup>. A vertical channel is formed by the vertically cross-stacked CNTs. The photocurrent mapping shows that the photocurrent is mainly produced at the cross point of the CNTs (Fig. 5(e)), confirming that the vertical channel exhibits higher carrier collection efficiency. As a result, high EQE of ~30% is achieved (Fig. 5(f)).

#### 2.4. 2D–3D heterojunction devices

Although strong light–matter interaction has been reported, the light absorption of 2D materials is still limited by the ultrathin characteristic, indirect bandgap and strong exciton binding energy<sup>[132, 133]</sup>, leading to unsatisfying photovoltaic performances. The self-passivated surface allows 2D materials to integrate with 3D bulk semiconductors through vdW interaction as well, which provides a solution for the limited optical absorption. Moreover, the mature CMOS technics is conducive to the on-chip integration of the devices. Thus, 2D–3D heterojunctions have attracted much attention on photovoltaics<sup>[134–136]</sup>.

2D materials/Si heterojunctions have been widely researched due to the high absorbance of Si and the compatibility with CMOS technics. In 2018, Xie *et al.* fabricated a multi-layered PtSe<sub>2</sub>/Si vertical hybrid heterojunction by selenylation of Pt films pre-deposited on Si substrates<sup>[137]</sup>. High photovoltaic performances with PCE of 8% and EQE of ~80% are achieved. The heterojunction also exhibits a good photoresponse over a wide spectrum ranging from 200 to 1550 nm, owing to the narrow bandgap of PtSe<sub>2</sub>. Moreover, the device is highly suitable for weak optical signal detection. In 2019, Wu *et al.* demonstrated a large-area 2D WS<sub>2</sub>/Si heterostructure<sup>[138]</sup>. Due to the facilitation of the photocarrier separation

process by the type-II band alignment, the fabricated device exhibits a photovoltaic effect with  $I_{SC}$  of  $5 \times 10^{-6}$  A. Remarkably, the heterostructure exhibits broadband photovoltaic response up to 3043 nm.

In 2018, Xiao *et al.* demonstrated a novel 2D/3D heterojunction of reduced graphene oxide (RGO)–MoS<sub>2</sub>/pyramid Si via solution-processing method (Fig. 6(a))<sup>[139]</sup>. As shown in Fig. 6(b), carriers are produced in the junction under illumination, and the RGO serves as a high-conductivity path for electrons that greatly facilitates the carrier transportation. Thus, the carrier collection efficiency is greatly enhanced. The  $I$ – $V$  characteristics of the device exhibits significant photovoltaic effect, where the  $V_{OC}$  and  $I_{SC}$  reach 300 mV and  $4 \times 10^2$   $\mu$ A, respectively (Fig. 6(c)). More importantly, the device also exhibits a broad-spectrum photovoltaic response, ranging from 350 nm to 4.3  $\mu$ m, which can be attributed to the decreased bandgap of MoS<sub>2</sub> caused by S vacancies.

Apart from Si, narrow-bandgap bulk semiconductors can be used for broadband photovoltaic devices, such as germanium (Ge) and HgCdTe (MCT). In 2020, a MoTe<sub>2</sub>/Ge heterojunction has been demonstrated by Chen *et al.*, showing prominent photovoltaic effect under 915-nm illumination<sup>[140]</sup>. As a narrow-bandgap material with excellent absorption, MCT is highly desired for the progress of photovoltaic devices. However, traditional MCT photovoltaic detectors exhibited low quantum efficiency due to the numerous interface defects caused by ion implantation<sup>[141]</sup>. To address this issue, Wang *et al.* fabricated a graphene/MCT heterojunction for uncooled mid-wave infrared (MWIR) photodetector in 2022<sup>[142]</sup>. By transferring high-mobility multilayer graphene onto MCT, a clean and defect-free interface is obtained (Fig. 6(d)). The device exhibits a pronounced photovoltaic effect in a wide spectrum region ranging from 520 to 4225 nm (Fig. 6(e)). It is

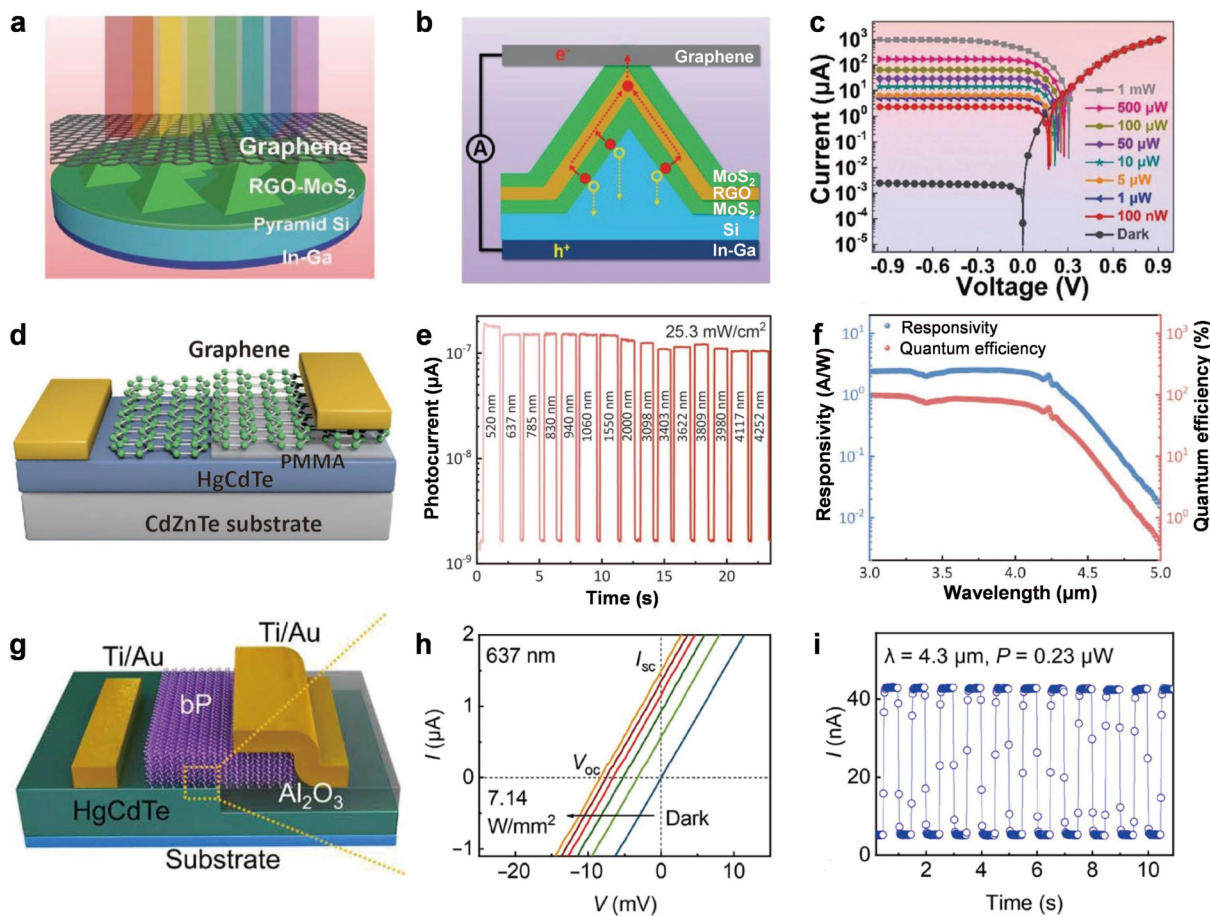


Fig. 6. (Color online) (a) Schematic of the RGO–MoS<sub>2</sub>/pyramid Si photodetector. (b) Schematic of the carrier transportation under illumination with RGO as high-conductivity path. (c)  $I$ – $V$  curves of the device under 808-nm laser with varied light powers. (a–c) Reproduced with permission<sup>[139]</sup>. Copyright 2018, Wiley-VCH. (d) Schematic of the vdWs-on-MCT photodetector at zero bias under varied wavelengths. (e)  $I$ – $T$  curve of the graphene/MCT photodetector. (d–f) Reproduced with permission<sup>[142]</sup>. Copyright 2021, Wiley-VCH. (g) Schematic of the HgCdTe/BP device. (h)  $I$ – $V$  curves of HgCdTe/BP device under 637-nm illumination. (i)  $I$ – $T$  curves of HgCdTe/BP device under 4.3- $\mu\text{m}$  light at zero bias. (g–i) Reproduced with permission<sup>[143]</sup>. Copyright 2022, American Association for the Advancement of Science.

worth noting that the blackbody radiation was investigated on vdW-on-MCT heterostructures. Fig. 6(f) shows a high quantum efficiency (85%) under blackbody radiation, which is comparable to those of commercial MWIR photodetectors in 3.8–4.8  $\mu\text{m}$  region.

In 2022, Jiao *et al.* also demonstrated a remarkable photovoltaic effect in the MCT/BP heterojunction (Fig. 6(g))<sup>[143]</sup>. Concretely, a broken-gap (type-III) band structure is obtained, forming a strong built-in electric field at the junction interface. A large photocurrent is obtained due to the photo-induced direct band-to-band tunneling (BTBT) mechanism (Fig. 6(h)). Owing to the high absorption in broadband, the heterojunction exhibits a good photovoltaic performance in a broad spectrum ranging from 520 to 4330 nm (Fig. 6(i)). Moreover, broadband polarization sensitivity without external optical elements is realized by the optical anisotropy of BP.

## 2.5. BPVE devices

The S–Q limit becomes a constraint on photovoltaic efficiency once a Schottky junction or a p–n junction is formed, where a built-in field is necessary<sup>[19, 144–147]</sup>. However, BPVE means no need of built-in field to generate photocurrent at zero bias. Thus, BPVE device has been considered as a promising candidate for surpassing the Shockley–Queisser (S–Q)

limit<sup>[148–150]</sup>. In the past few years, various 3D ferroelectric materials have boosted studies on BPVE. Most of these ferroelectric materials are insulators, such as barium titanate ( $\text{BaTiO}_3$ ) and bismuth iron oxide ( $\text{BiFeO}_3$ ), where the photocurrent density is fundamentally limited by the large bandgap (2.7–5 eV)<sup>[151, 152]</sup>. BPVE has also been discovered in 2D materials with broken inversion symmetry<sup>[153]</sup>. Recent studies have shown that BPVE in 2D materials can achieve higher photocurrent conversion efficiency than 3D crystal structures do<sup>[145, 146, 151–154]</sup>. Moreover, the unique properties such as dangling-bond-free surface and flexibility allow 2D materials to realize BPVE by symmetry engineering, such as fabricating vdW interface and nanotubes.

BPVE in ferroelectric 2D materials, such as  $\text{In}_2\text{Se}_3$  and  $\text{CuInP}_2\text{S}_6$  (CIPS), has been predicted and experimentally demonstrated<sup>[154]</sup>. In 2021, Li *et al.* fabricated CIPS-based photovoltaic device, where the ultra-thin CIPS is sandwiched by the graphene electrodes (Fig. 7(a))<sup>[155]</sup>. The device exhibits a prominent photovoltaic behavior, with a short-circuit current density ( $J_{sc}$ ) up to  $10 \text{ mA}\cdot\text{cm}^{-2}$ , which is significantly higher than conventional bulk ferroelectric materials. In addition, the BPVE in CIPS-based devices can be modulated by varying the external electric field, which can be explained by

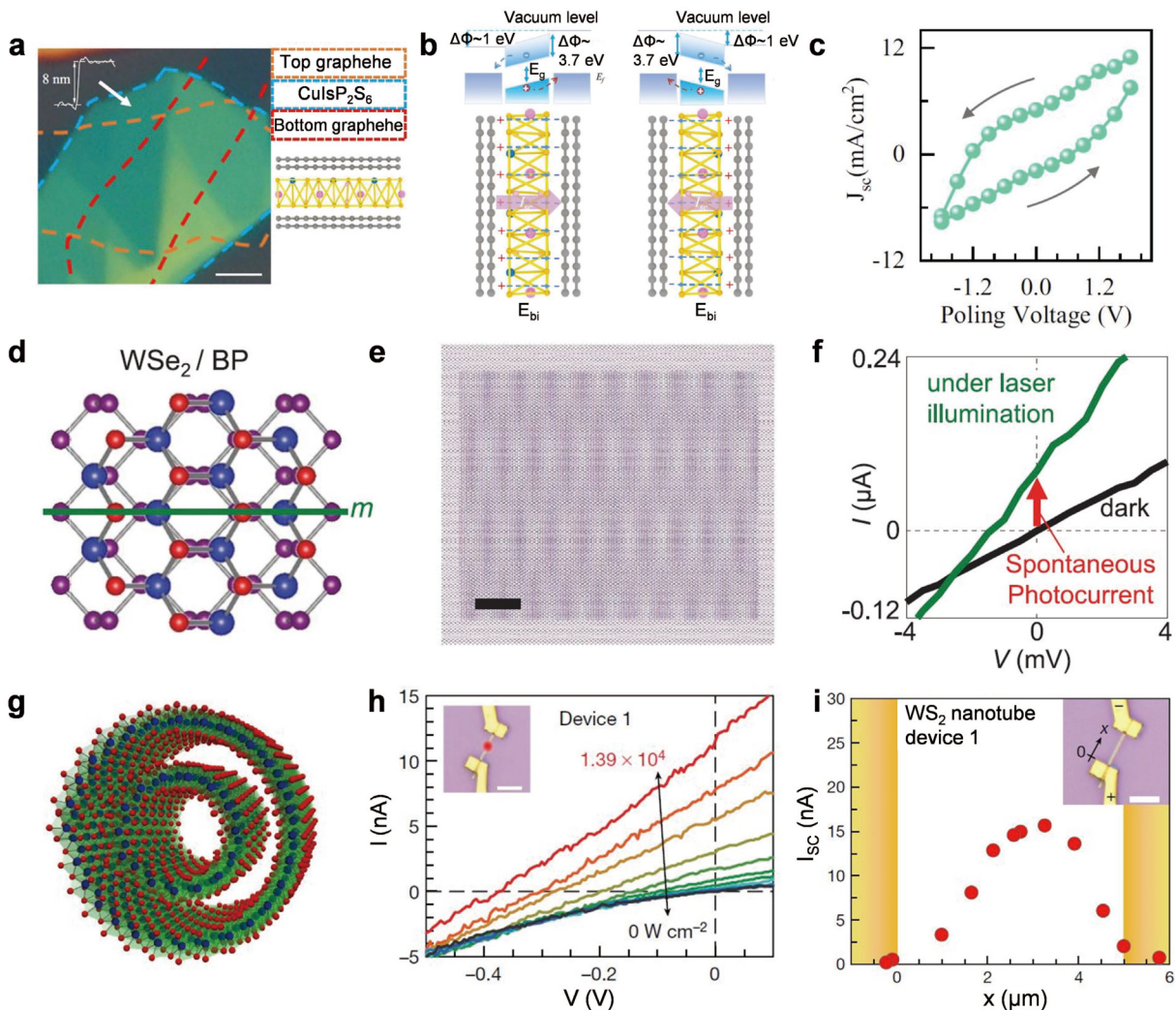


Fig. 7. (Color online) (a) The optical image of the 2D CIPS BPVE device. (b) The band alignment of the graphene/CIPS/graphene heterojunction at different polarization state of CIPS. (c) The plot of  $J_{SC}$  as a function of the poling voltage. (a–c) Reproduced with permission<sup>[155]</sup>. Copyright 2021, Springer Nature. (d) Schematic of the WSe<sub>2</sub>/BP heterointerface. (e) Moiré patterns of the WSe<sub>2</sub>/BP heterojunction when the mirror planes of BP and WSe<sub>2</sub> are parallel. (f)  $I$ – $V$  curves of the WSe<sub>2</sub>/BP device. (d–f) Reproduced with permission<sup>[156]</sup>. Copyright 2021, American Association for the Advancement of Science. (g) Schematic of the crystal structure of a WS<sub>2</sub> multiwall nanotube. (h)  $I$ – $V$  curves under 632.8 nm laser with varied light powers. Inset, optical image of the device. (i) The  $I_{SC}$  versus position of the laser spot in the nanotube device. (g–i) Reproduced with permission<sup>[159]</sup>. Copyright 2019, Springer Nature.

the tunable band alignment in the heterostructure device (Fig. 7(b)). The off-center shift of the Cu ions in CIPS results in out-of-plane ferroelectricity, and the generation of an internal electric field ( $E_{bi}$ ) lead to different band alignment of graphene at different electrode interfaces (i.e., asymmetric energy potential barrier height  $\Delta\Phi$ ). Under illumination, the carriers are separated by  $E_{bi}$  and drifted under  $\Delta\Phi$ . Notably, the direction of the photocurrent is switchable due to the controllable electric polarization. Asymmetric photocurrent is observed due to the ferroelectric hysteresis of CIPS, confirmed by the extracted  $J_{SC}$  at each poling voltage, where the  $J_{SC}$  follows an obvious hysteresis loop (Fig. 7(c)).

In addition to photoferroic devices, the intentional disruption of in-plane inversion symmetry in vdW heterojunctions can also lead to BPVE. In 2021, Akamatsu *et al.* designed a WSe<sub>2</sub>/BP heterojunction by stacking crystals with different rotational symmetries at specific angle to reduce the interfacial symmetry, showing prominent in-plane electronic polarization<sup>[156]</sup>. Owing to the threefold rotation symmetry of WSe<sub>2</sub>, being mismatched with the twofold rotational symmetry of

BP, the interface of BP and WSe<sub>2</sub> exhibits no rotational symmetry (Fig. 7(d)). And the mirror symmetry remains when the mirror planes of BP and WSe<sub>2</sub> are parallel, resulting in electronic polarization along the parallel direction of the mirror plane, and the photocurrent appears along the polarization direction. The stripe moiré pattern is observed due to the lattice mismatch between WSe<sub>2</sub> and BP, reflecting the in-plane polarity at the WSe<sub>2</sub>/BP junction interface (Fig. 7(e)). As shown in Fig. 7(f), a large  $I_{SC}$  is observed under illumination, indicating a significant BPVE characteristic. Furthermore, by measuring the direction dependent photocurrent, it is confirmed that the direction of photocurrent generation and polarization are both parallel to the mirror direction. The results provide a strategy for symmetry engineering of various vdW interfaces.

The BPVE can also be observed in 2D TMDs when the inherent inversion symmetry is broken. When the mirror symmetries and threefold rotational of the 2D materials are broken due to bending or strain, BPVE can be realized, facilitating the research on 1D-nanotubes and flexo-photovoltaic-based devices<sup>[157–159]</sup>. In 2019, Zhang *et al.* fabricated WS<sub>2</sub>

devices based on non-centrosymmetric polar nanotubes with a hollow core (Fig. 7(g))<sup>[19]</sup>. As shown in Fig. 7(h), the  $I_{SC}$  and  $V_{OC}$  both monotonically vary with laser power, confirming the occurrence of BPVE. It is found that the reduction of crystal symmetry by moving from a 2D monolayer WS<sub>2</sub> to a polar tubular WS<sub>2</sub> can greatly enhance the BPVE. The  $I_{SC}$  of WS<sub>2</sub> nanotube devices (Fig. 7(i)) is significantly larger than that of the monolayer WS<sub>2</sub> devices. Thus, reducing the crystal symmetry is essential for BPVE. In addition, the flexo-photo voltaic effect (FPVE) is a strain-gradient-induced BPVE which represents the photocurrent response caused by the symmetry breaking of asymmetric crystals. Jiang *et al.* proposed a strain-gradient engineering approach based on structural heterogeneity and phase transition of a MoS<sub>2</sub> and VO<sub>2</sub> hybrid system, demonstrating the FPVE in the MoS<sub>2</sub><sup>[147]</sup>. Prominent  $I_{SC}$  is observed under illumination, and the bulk photovoltaic coefficient of the MoS<sub>2</sub> is significantly larger than that in most non-centrosymmetric materials. The FPVE discovered in 2D materials leads to a new guidance in potential photovoltaic applications.

### 3. Conclusion and outlook

2D materials have shown great potential in photovoltaic devices owing to the unique optoelectronic properties, including broadband light absorption, strong light–matter interaction, and flexibility. Moreover, the self-passivated surface allows the fabrication of devices through vdW interaction without the lattice mismatch, such as vdW metal contact and vdW p–n heterojunction. On this basis, band engineering can be realized and the photovoltaic performances such as EQE, PCE and  $V_{OC}$  can be significantly enhanced. In this review, we have presented the recent advances in photovoltaic devices based on 2D materials, including Schottky junctions, homojunctions, 2D–2D heterojunctions, 2D–3D heterojunctions, and BPVE devices.

2D Schottky junctions based on vdW metal contact have shown great advantages in photovoltaic devices. The vdW metal contact leads to defect-free interface without the Fermi-level pinning, so that large built-in field and wide depletion width can be obtained, and the defect-induced recombination loss is also impeded. Therefore, the photovoltaic performance can be greatly enhanced. Moreover, vertical contact device reduces the carrier recombination loss during the transportation, further improving the photovoltaic performances. 2D homojunctions can be realized by doping and external field modulation. Doping provides a feasible way for fabricating p–n homojunctions, and multiple strategies such as plasma doping, ion exchanging doping and solid-state doping have been successfully applied in photovoltaic devices. The external field enables effective and reconfigurable modulation of carrier transportation in 2D materials to realize the p–n homojunctions, and the photovoltaic performances of the p–n homojunctions can be improved by the modulation. Novel strategies such as reversible solid-state doping have also been developed in recent years. P–n heterojunctions with different 2D materials can be easily fabricated through vdW interaction, which provide a new pathway for band engineering for high-performance photovoltaics. Strategies for fabricating heterojunctions such as unilateral depletion, excitonic photovoltaic effect, combination with high-absorption

Table 2. Performance comparison of representative works in recent years.

Devices	PCE (%)	EQE (%)	$V_{OC}$ (V)	FF	References
Pt/MoS <sub>2</sub> /Ag	0.2	1.74	1.02	0.26	[82]
1T'-MoTe <sub>2</sub> /MoS <sub>2</sub> /Cr	–	20	0.19	–	[83]
WS <sub>2</sub> /Au	0.46	40	0.256	0.44	[84]
Gr/WS <sub>2</sub> /Pt	5	92	0.4	0.39	[86]
Gr/WO <sub>x</sub> /WSe <sub>2</sub> /Pt	5.44	–	0.47	0.59	[87]
MoO <sub>x</sub> /Gr/WSe <sub>2</sub> /Au	5.1	–	0.476	0.617	[88]
MoTe <sub>2</sub> homojunction	–	40	0.3	0.5	[107]
WSe <sub>2</sub> homojunction	–	83.6	0.75	–	[106]
CsPbBr <sub>3</sub> /CdS	17.5	–	0.76	0.5	[122]
Cs <sub>2</sub> AgBiBr <sub>6</sub> /WS <sub>2</sub> /Gr	–	14.7	–	–	[127]
Gr/WSe <sub>2</sub> /MoS <sub>2</sub>	3.4	50	0.38	–	[85]
PbS/MoS <sub>2</sub> /WSe <sub>2</sub>	7.65	100	0.42	–	[123]
Perovskite/BP/MoS <sub>2</sub>	–	80	0.32	–	[128]
MoS <sub>2</sub> /AsP	9	71	0.61	0.5	[121]
Gr/WO <sub>x</sub> /WSe <sub>2</sub> //MoS <sub>2</sub>	5	–	0.46	0.45	[129]
CNT/WSe <sub>2</sub> /MoS <sub>2</sub> /CNT	–	42.7	0.35	–	[131]
PtSe <sub>2</sub> /Si	–	80	0.3	–	[137]

materials, contact engineering, and vertical carrier transportation have been demonstrated to realize high-performance photovoltaic devices. 2D–3D p–n heterojunctions utilize the advantage of conventional bulk semiconductors, such as large optical absorption and broadband absorption, which effectively overcome the limited absorption in 2D materials. The p–n heterojunctions using Si and Ge exhibit large light absorption. Moreover, the p–n heterojunctions using narrow-bandgap materials such as HgCdTe exhibit broadband absorption. BPVE has been discovered in 2D materials and demonstrated to be promising for overcoming the S–Q limit. BPVE can be realized in non-centrosymmetric 2D materials, and by symmetry engineering such as fabricating vdW interface and fabricating nanotubes. Table 2 shows the performance comparison of representative works in recent years.

In spite of the great progress achieved, the photovoltaic devices based on 2D materials are still facing some challenges. Fig. 8 shows the outlooks on the future development of 2D photovoltaic devices.

On the one hand, the performances of 2D photovoltaic devices need further improvement. The PCEs of most currently reported 2D photovoltaic devices are below 5%, showing large gap from the theoretical limit<sup>[160]</sup>. Extensive researches have been focused on improving the EQE and  $I_{SC}$ . However,  $V_{OC}$  is also a key parameter for realizing high PCE. Currently the most reported  $V_{OC}$  values of 2D photovoltaic devices are below 0.5 V, while the bandgaps of most 2D semiconductors are in the range of 1–2 eV<sup>[133, 161–163]</sup>, indicating that there is still significant room to improve the  $V_{OC}$ . The key to address the low  $V_{OC}$  lies in modulation of the built-in field. Doping can effectively modulate the built-in field by modulating the doping concentration. However, realizing controllable doping while maintaining good stability and high carrier mobility remains a great challenge. Novel doping methods need further development, such as solid-state doping and remote modulation doping<sup>[58, 164]</sup>. Contact engineering can modulate the carrier transportation at the interface. By reducing the carrier recombination and extra Schottky bar-

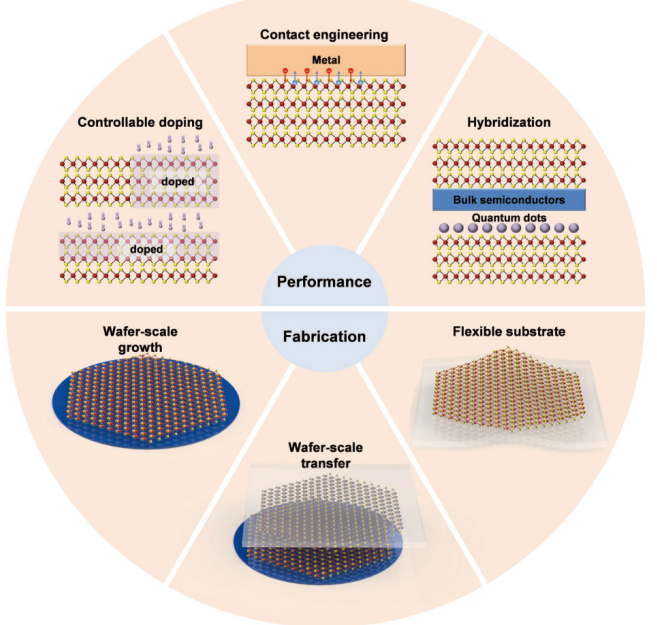


Fig. 8. (Color online) Outlooks on the future development of 2D photovoltaic devices.

rier, the  $V_{OC}$  and PCE can be improved<sup>[83, 87, 129]</sup>. However, the currently developed methods exhibit limited performances. Novel strategies such as semi-metal contact with strong van der Waals interaction have pushed the carrier transportation to the theoretical limit, which can be further employed in photovoltaics<sup>[165]</sup>. The low-absorption efficiency is also a challenge limiting the  $V_{OC}$  and PCE. The most 2D materials exhibit indirect bandgap and large exciton binding energy, which limit the optical absorption. The hybridization of 2D materials with large-optical-absorption materials has been demonstrated effective for improving the photovoltaic performance, such as the hybridization with bulk semiconductors and quantum dots.

On the other hand, the fabrication of large-scale 2D photovoltaic devices is a key challenge for the practical application. First, high-quality and controllable wafer-scale synthesis of 2D materials and vdW heterojunctions still faces great challenges. Currently, only a few wafer-scale 2D materials have been reported<sup>[112, 166–168]</sup>. Yet more 2D materials are needed for high-performance photovoltaic devices, such as WSe<sub>2</sub> and black phosphorus. And the quality of wafer-scale single crystal also needs improvement. Second, wafer-scale transfer is vital for fabricating photovoltaic devices with p–n junctions or Schottky junctions. Wafer-scale transfer have been demonstrated in graphene and metals recently<sup>[169, 170]</sup>, and could be further extended to other 2D semiconductors to fabricate large-scale photovoltaic devices. Last but not least, the flexibility of 2D materials provides great opportunity for flexible and wearable devices. And the research on the integration of large-scale 2D photovoltaic devices on flexible substrates is in desperate need for the practical application.

In conclusion, 2D materials are promising for next-generation high-performance photovoltaic devices, and great achievements have been made in recent years. To further push the practical application of 2D photovoltaic devices, novel strategies for improving the performances and technologies for large-scale fabrication need further development.

## Acknowledgments

This work was supported by the National Natural Science Foundation of China (52322210, 52172144, 22375069, 21825103, and U21A2069), National Key R&D Program of China (2021YFA1200501), Shenzhen Science and Technology Program (JCYJ20220818102215033, JCYJ20200109105422876) and the Innovation Project of Optics Valley Laboratory (OVL2023PY007).

## References

- [1] Liu W Z, Liu Y J, Yang Z Q, et al. Flexible solar cells based on foldable silicon wafers with blunted edges. *Nature*, 2023, **617**, 717
- [2] Wu X M, Gao C S, Chen Q Z, et al. High-performance vertical field-effect organic photovoltaics. *Nat Commun*, 2023, **14**, 1579
- [3] Chu X B, Ye Q F, Wang Z H, et al. Surface in situ reconstruction of inorganic perovskite films enabling long carrier lifetimes and solar cells with 21% efficiency. *Nat Energy*, 2023, **8**, 372
- [4] Yang T H, Gao L L, Lu J, et al. One-stone-for-two-birds strategy to attain beyond 25% perovskite solar cells. *Nat Commun*, 2023, **14**, 839
- [5] Ji R, Zhang Z B, Hofstetter Y J, et al. Perovskite phase heterojunction solar cells. *Nat Energy*, 2022, **7**, 1170
- [6] Polman A, Knight M, Garnett E C, et al. Photovoltaic materials: Present efficiencies and future challenges. *Science*, 2016, **352**, aad4424
- [7] Kublitski J, Hofacker A, Boroujeni B K, et al. Reverse dark current in organic photodetectors and the major role of traps as source of noise. *Nat Commun*, 2021, **12**, 551
- [8] Sakhatsky I, Turedi B, Matt G J, et al. Stable perovskite single-crystal X-ray imaging detectors with single-photon sensitivity. *Nat Photonics*, 2023, **17**, 510
- [9] Sun Y, Xu S T, Xu Z Q, et al. Mesoscopic sliding ferroelectricity enabled photovoltaic random access memory for material-level artificial vision system. *Nat Commun*, 2022, **13**, 5391
- [10] Pi L J, Wang P F, Liang S J, et al. Broadband convolutional processing using band-alignment-tunable heterostructures. *Nat Electron*, 2022, **5**, 248
- [11] Liu K L, Jin B, Han W, et al. A wafer-scale van der Waals dielectric made from an inorganic molecular crystal film. *Nat Electron*, 2021, **4**, 906
- [12] Liu Y, Huang Y, Duan X F. Van der Waals integration before and beyond two-dimensional materials. *Nature*, 2019, **567**, 323
- [13] Jariwala D, Marks T J, Hersam M C. Mixed-dimensional van der Waals heterostructures. *Nat Mater*, 2017, **16**, 170
- [14] Shu Z W, Peng Q J, Huang P, et al. Growth of ultrathin ternary teallite (PbSnS<sub>2</sub>) flakes for highly anisotropic optoelectronics. *Matter*, 2020, **2**, 977
- [15] Liang S J, Cheng B, Cui X Y, et al. Van der Waals heterostructures for high-performance device applications: Challenges and opportunities. *Adv Mater*, 2020, **32**, 1903800
- [16] Xu Y S, Liu T, Liu K L, et al. Scalable integration of hybrid high- $\kappa$  dielectric materials on two-dimensional semiconductors. *Nat Mater*, 2023, **22**, 1078
- [17] Britnell L, Ribeiro R M, Eckmann A, et al. Strong light-matter interactions in heterostructures of atomically thin films. *Science*, 2013, **340**, 1311
- [18] Lukman S, Ding L, Xu L, et al. High oscillator strength interlayer excitons in two-dimensional heterostructures for mid-infrared photodetection. *Nat Nanotechnol*, 2020, **15**, 675
- [19] Zhang Y J, Ideue T, Onga M, et al. Enhanced intrinsic photovoltaic effect in tungsten disulfide nanotubes. *Nature*, 2019, **570**, 349
- [20] Chen Y F, Wang Y, Wang Z, et al. Unipolar barrier photodetectors based on van der Waals heterostructures. *Nat Electron*, 2021, **4**, 357

- [21] Huo N, Gupta S, Konstantatos G. MoS<sub>2</sub>-HgTe quantum dot hybrid photodetectors beyond 2 μm. *Adv Mater*, 2017, 29, 1606576
- [22] Krishnamurthi V, Khan H, Ahmed T, et al. Liquid-metal synthesized ultrathin SnS layers for high-performance broadband photodetectors. *Adv Mater*, 2020, 32, 2004247
- [23] Zhou X, Hu X Z, Zhou S S, et al. Tunneling diode based on WSe<sub>2</sub>/SnS<sub>2</sub> heterostructure incorporating high detectivity and responsivity. *Adv Mater*, 2018, 30, 1703286
- [24] Zhou X, Gan L, Tian W M, et al. Ultrathin SnSe<sub>2</sub> flakes grown by chemical vapor deposition for high-performance photodetectors. *Adv Mater*, 2015, 27, 8035
- [25] Lv L, Zhuge F W, Xie F J, et al. Reconfigurable two-dimensional optoelectronic devices enabled by local ferroelectric polarization. *Nat Commun*, 2019, 10, 3331
- [26] Buscema M, Island J O, Groenendijk D J, et al. Photocurrent generation with two-dimensional van der Waals semiconductors. *Chem Soc Rev*, 2015, 44, 3691
- [27] Xia F F, Wang F K, Hu H L, et al. Application of second harmonic generation in characterization of 2D materials. *J Inorg Mater*, 2021, 36, 1022
- [28] Liu G H, Sun Z D, Su J W, et al. Preparation and photodetection performance of two-dimensional In<sub>2/3</sub>PSe<sub>3</sub> nanosheets. *Chin Sci Bull*, 2021, 66, 4036
- [29] Qiu Q X, Huang Z M. Photodetectors of 2D materials from ultraviolet to terahertz waves. *Adv Mater*, 2021, 33, 2008126
- [30] Liu W, Lv J H, Peng L, et al. Graphene charge-injection photodetectors. *Nat Electron*, 2022, 5, 281
- [31] Gao A Y, Lai J W, Wang Y J, et al. Observation of ballistic avalanche phenomena in nanoscale vertical InSe/BP heterostructures. *Nat Nanotechnol*, 2019, 14, 217
- [32] Tong L, Huang X Y, Wang P, et al. Stable mid-infrared polarization imaging based on quasi-2D tellurium at room temperature. *Nat Commun*, 2020, 11, 2308
- [33] Peng M, Xie R Z, Wang Z, et al. Blackbody-sensitive room-temperature infrared photodetectors based on low-dimensional tellurium grown by chemical vapor deposition. *Sci Adv*, 2021, 7, eabf7358
- [34] Long M S, Wang Y, Wang P, et al. Palladium diselenide long-wavelength infrared photodetector with high sensitivity and stability. *ACS Nano*, 2019, 13, 2511
- [35] Luo L B, Wang D, Xie C, et al. PdSe<sub>2</sub> multilayer on germanium nanocones array with light trapping effect for sensitive infrared photodetector and image sensing application. *Adv Funct Mater*, 2019, 29, 1900849
- [36] Pi L J, Hu C G, Shen W F, et al. Highly in-plane anisotropic 2D PdSe<sub>2</sub> for polarized photodetection with orientation selectivity. *Adv Funct Mater*, 2021, 31, 2006774
- [37] Wang Z, Wang P, Wang F, et al. A noble metal dichalcogenide for high-performance field-effect transistors and broadband photodetectors. *Adv Funct Mater*, 2020, 30, 1907945
- [38] Wu D, Jia C, Shi F H, et al. Mixed-dimensional PdSe<sub>2</sub>/SiNWA heterostructure based photovoltaic detectors for self-driven, broadband photodetection, infrared imaging and humidity sensing. *J Mater Chem A*, 2020, 8, 3632
- [39] Wu D, Wang Y G, Zeng L H, et al. Design of 2D layered PtSe<sub>2</sub> heterojunction for the high-performance, room-temperature, broadband, infrared photodetector. *ACS Photonics*, 2018, 5, 3820
- [40] Luo S Y, Peng L, Xie Y S, et al. Flexible large-area graphene films of 50–600 nm thickness with high carrier mobility. *Nano-Micro Lett*, 2023, 15, 61
- [41] Wang Y H, Pang J B, Cheng Q L, et al. Applications of 2D-layered palladium diselenide and its van der Waals heterostructures in electronics and optoelectronics. *Nano-Micro Lett*, 2021, 13, 143
- [42] Du J L, Yu H H, Liu B S, et al. Strain engineering in 2D material-based flexible optoelectronics. *Small Methods*, 2021, 5, 2000919
- [43] Akinwande D, Petrone N, Hone J. Two-dimensional flexible nanoelectronics. *Nat Commun*, 2014, 5, 5678
- [44] Yu J D, Wang L, Hao Z B, et al. Van der Waals epitaxy of III-nitride semiconductors based on 2D materials for flexible applications. *Adv Mater*, 2020, 32, 1903407
- [45] Withers F, Del Pozo-Zamudio O, Mishchenko A, et al. Light-emitting diodes by band-structure engineering in van der Waals heterostructures. *Nat Mater*, 2015, 14, 301
- [46] Cai S, Xu X J, Yang W, et al. Materials and designs for wearable photodetectors. *Adv Mater*, 2019, 31, 1808138
- [47] Chang T H, Li K R, Yang H T, et al. Multifunctionality and mechanical actuation of 2D materials for skin-mimicking capabilities. *Adv Mater*, 2018, 30, 1802418
- [48] Li Z W, Lv Y W, Ren L W, et al. Efficient strain modulation of 2D materials via polymer encapsulation. *Nat Commun*, 2020, 11, 1151
- [49] Wang H Y, Li Z X, Li D Y, et al. Van der Waals integration based on two-dimensional materials for high-performance infrared photodetectors. *Adv Funct Mater*, 2021, 31, 2103106
- [50] Liang Q J, Wang Q X, Zhang Q, et al. High-performance, room temperature, ultra-broadband photodetectors based on air-stable PdSe<sub>2</sub>. *Adv Mater*, 2019, 31, 1807609
- [51] Long M S, Gao A Y, Wang P, et al. Room temperature high-detectivity mid-infrared photodetectors based on black arsenic phosphorus. *Sci Adv*, 2017, 3, e1700589
- [52] Qiao H, Yuan J, Xu Z Q, et al. Broadband photodetectors based on graphene-Bi<sub>2</sub>Te<sub>3</sub> heterostructure. *ACS Nano*, 2015, 9, 1886
- [53] Geim A K, Grigorieva I V. Van der Waals heterostructures. *Nature*, 2013, 499, 419
- [54] Wang F K, Luo P, Zhang Y, et al. Band structure engineered tunneling heterostructures for high-performance visible and near-infrared photodetection. *Sci China Mater*, 2020, 63, 1537
- [55] Cao Y M, Stavrinadis A, Lasanta T, et al. The role of surface passivation for efficient and photostable PbS quantum dot solar cells. *Nat Energy*, 2016, 1, 16035
- [56] Fiducia T A M, Mendis B G, Li K X, et al. Understanding the role of selenium in defect passivation for highly efficient selenium-alloyed cadmium telluride solar cells. *Nat Energy*, 2019, 4, 504
- [57] Zhou Y, Wang L, Chen S Y, et al. Thin-film Sb<sub>2</sub>Se<sub>3</sub> photovoltaics with oriented one-dimensional ribbons and benign grain boundaries. *Nat Photonics*, 2015, 9, 409
- [58] Lee S J, Lin Z Y, Huang J, et al. Programmable devices based on reversible solid-state doping of two-dimensional semiconductors with superionic silver iodide. *Nat Electron*, 2020, 3, 630
- [59] Seo S Y, Moon G, Okello O F N, et al. Reconfigurable photo-induced doping of two-dimensional van der Waals semiconductors using different photon energies. *Nat Electron*, 2021, 4, 38
- [60] Avsar A, Marinov K, Marin E G, et al. Reconfigurable diodes based on vertical WSe<sub>2</sub> transistors with van der Waals bonded contacts. *Adv Mater*, 2018, 30, 1707200
- [61] Resta G V, Balaji Y, Lin D, et al. Doping-free complementary logic gates enabled by two-dimensional polarity - controllable transistors. *ACS Nano*, 2018, 12, 7039
- [62] Luo W, Zhu M J, Peng G, et al. Carrier modulation of ambipolar few-layer MoTe<sub>2</sub> transistors by MgO surface charge transfer doping. *Adv Funct Mater*, 2018, 28, 1704539
- [63] Qu D S, Liu X C, Huang M, et al. Carrier-type modulation and mobility improvement of thin MoTe<sub>2</sub>. *Adv Mater*, 2017, 29, 1606433
- [64] Wang F K, Wu J, Zhang Y, et al. High-sensitivity shortwave infrared photodetectors of metal-organic frameworks integrated on 2D layered materials. *Sci China Mater*, 2022, 65, 451
- [65] Tan C L, Cao X H, Wu X J, et al. Recent advances in ultrathin two-dimensional nanomaterials. *Chem Rev*, 2017, 117, 6225
- [66] Wang X T, Cui Y, Li T, et al. Recent advances in the functional 2D photonic and optoelectronic devices. *Adv Opt Mater*, 2019, 7, 1801274

- [67] Huo N, Konstantatos G. Recent progress and future prospects of 2D-based photodetectors. *Adv Mater*, 2018, 30, 1801164
- [68] Zhang L, Han X N, Zhang S H, et al. Gate-tunable photovoltaic behavior and polarized image sensor based on all-2D TaIrTe<sub>4</sub>/MoS<sub>2</sub> van der Waals Schottky diode. *Adv Electron Mater*, 2022, 8, 2200551
- [69] Luo M, Wu F, Long M S, et al. WSe<sub>2</sub>/Au vertical Schottky junction photodetector with low dark current and fast photoresponse. *Nanotechnology*, 2018, 29, 444001
- [70] McVay E, Zubair A, Lin Y X, et al. Impact of Al<sub>2</sub>O<sub>3</sub> passivation on the photovoltaic performance of vertical WSe<sub>2</sub> Schottky junction solar cells. *ACS Appl Mater Interfaces*, 2020, 12, 57987
- [71] Han J F, Fang C C, Yu M, et al. A high-performance Schottky photodiode with asymmetric metal contacts constructed on 2D Bi<sub>2</sub>O<sub>2</sub>Se. *Adv Electron Mater*, 2022, 8, 2100987
- [72] Zhao Z J, Rakheja S, Zhu W J. Nonvolatile reconfigurable 2D schottky barrier transistors. *Nano Lett*, 2021, 21, 9318
- [73] Schulman D S, Arnold A J, Das S. Contact engineering for 2D materials and devices. *Chem Soc Rev*, 2018, 47, 3037
- [74] Mleczko M J, Yu A C, Smyth C M, et al. Contact engineering high-performance n-type MoTe<sub>2</sub> transistors. *Nano Lett*, 2019, 19, 6352
- [75] Zhang Y, Yin L, Chu J W, et al. Edge-epitaxial growth of 2D NbS<sub>2</sub>-WS<sub>2</sub> lateral metal-semiconductor heterostructures. *Adv Mater*, 2018, 30, 1803665
- [76] Huo J P, Zou G S, Xiao Y, et al. High performance 1D-2D CuO/MoS<sub>2</sub> photodetectors enhanced by femtosecond laser-induced contact engineering. *Mater Horiz*, 2023, 10, 524
- [77] Lian W T, Cao R, Li G, et al. Distinctive deep-level defects in non-stoichiometric Sb<sub>2</sub>Se<sub>3</sub> photovoltaic materials. *Adv Sci*, 2022, 9, 2105268
- [78] Hassan A, Wang Z J, Ahn Y H, et al. Recent defect passivation drifts and role of additive engineering in perovskite photovoltaics. *Nano Energy*, 2022, 101, 107579
- [79] Su R, Xu Z J, Wu J, et al. Dielectric screening in perovskite photovoltaics. *Nat Commun*, 2021, 12, 2479
- [80] Gan J, Yu M, Hoye R L Z, et al. Defects, photophysics and passivation in Pb-based colloidal quantum dot photovoltaics. *Mater Today Nano*, 2021, 13, 100101
- [81] Xu B, Qin X T, Lin J J, et al. Positive role of inhibiting CZTSSe decomposition on intrinsic defects and interface recombination of 12.03% efficient kesterite solar cells. *Sol RRL*, 2022, 6, 2200256
- [82] Liu Y, Guo J, Zhu E B, et al. Approaching the Schottky-Mott limit in van der Waals metal-semiconductor junctions. *Nature*, 2018, 557, 696
- [83] Zhang X K, Liu B S, Gao L, et al. Near-ideal van der Waals rectifiers based on all-two-dimensional Schottky junctions. *Nat Commun*, 2021, 12, 1522
- [84] Went C M, Wong J, Jahelka P R, et al. A new metal transfer process for van der Waals contacts to vertical Schottky-junction transition metal dichalcogenide photovoltaics. *Sci Adv*, 2019, 5, eaax6061
- [85] Wong J, Jariwala D, Tagliabue G, et al. High photovoltaic quantum efficiency in ultrathin van der Waals heterostructures. *ACS Nano*, 2017, 11, 7230
- [86] Wang H Y, Wang W, Zhong Y L, et al. Approaching the external quantum efficiency limit in 2D photovoltaic devices. *Adv Mater*, 2022, 34, 2206122
- [87] Kim K H, Andreev M, Choi S, et al. High-efficiency WSe<sub>2</sub> photovoltaic devices with electron-selective contacts. *ACS Nano*, 2022, 16, 8827
- [88] Nazif K N, Daus A, Hong J H, et al. High-specific-power flexible transition metal dichalcogenide solar cells. *Nat Commun*, 2021, 12, 7034
- [89] Wu G J, Tian B B, Liu L, et al. Programmable transition metal dichalcogenide homojunctions controlled by nonvolatile ferroelectric domains. *Nat Electron*, 2020, 3, 43
- [90] Hu Z H, Wu Z T, Han C, et al. Two-dimensional transition metal dichalcogenides: interface and defect engineering. *Chem Soc Rev*, 2018, 47, 3100
- [91] Cui F F, Feng Q L, Hong J H, et al. Synthesis of large-size 1T' ReS<sub>2x</sub>Se<sub>2(1-x)</sub> alloy monolayer with tunable bandgap and carrier type. *Adv Mater*, 2017, 29, 1705015
- [92] Pang C S, Chen C Y, Ameen T, et al. WSe<sub>2</sub> homojunction devices: Electrostatically configurable as diodes, MOSFETs, and tunnel FETs for reconfigurable computing. *Small*, 2019, 15, 1902770
- [93] Wu B M, Wang X D, Tang H W, et al. Multifunctional MoS<sub>2</sub> transistors with electrolyte gel gating. *Small*, 2020, 16, 2000420
- [94] Li K J, He T, Guo N, et al. Light-triggered and polarity-switchable homojunctions for optoelectronic logic devices. *Adv Opt Mater*, 2023, 11, 2202379
- [95] Wang F K, Pei K, Li Y, et al. 2D homojunctions for electronics and optoelectronics. *Adv Mater*, 2021, 33, 2005303
- [96] Shan Y F, Yin Z W, Zhu J Q, et al. Few-layered MoS<sub>2</sub> based vertical van der Waals p-n homojunction by highly-efficient N<sub>2</sub> plasma implantation. *Adv Electron Mater*, 2022, 8, 2200299
- [97] Sun J C, Wang Y Y, Guo S Q, et al. Lateral 2D WSe<sub>2</sub> p-n homojunction formed by efficient charge-carrier-type modulation for high-performance optoelectronics. *Adv Mater*, 2020, 32, 1906499
- [98] He Q Y, Liu Y, Tan C L, et al. Quest for p-type two-dimensional semiconductors. *ACS Nano*, 2019, 13, 12294
- [99] Carozo V, Wang Y X, Fujisawa K, et al. Optical identification of sulfur vacancies: Bound excitons at the edges of monolayer tungsten disulfide. *Sci Adv*, 2017, 3, e1602813
- [100] Li Z X, Li D Y, Wang H Y, et al. Universal p-type doping via lewis acid for 2D transition-metal dichalcogenides. *ACS Nano*, 2022, 16, 4884
- [101] Liu Y D, Cai Y Q, Zhang G, et al. Al-doped black phosphorus p-n homojunction diode for high performance photovoltaic. *Adv Funct Mater*, 2017, 27, 1604638
- [102] Kim D K, Hong S B, Jeong K, et al. P-N junction diode using plasma boron-doped black phosphorus for high-performance photovoltaic devices. *ACS Nano*, 2019, 13, 1683
- [103] Li Y B, Xiao J C, Cao X Q, et al. Lateral WSe<sub>2</sub> homojunction through metal contact doping: Excellent self-powered photovoltaic photodetector. *Adv Funct Mater*, 2023, 33, 2213385
- [104] Zhang Y W, Ma K K, Zhao C, et al. An ultrafast WSe<sub>2</sub> photodiode based on a lateral p-i-n homojunction. *ACS Nano*, 2021, 15, 4405
- [105] Lee H S, Lim J Y, Yu S, et al. Seamless MoTe<sub>2</sub> homojunction PIN diode toward 1300 nm short-wave infrared detection. *Adv Opt Mater*, 2019, 7, 1900768
- [106] Chen P, Atallah T L, Lin Z Y, et al. Approaching the intrinsic exciton physics limit in two-dimensional semiconductor diodes. *Nature*, 2021, 599, 404
- [107] Wu G J, Wang X D, Chen Y, et al. MoTe<sub>2</sub> p-n homojunctions defined by ferroelectric polarization. *Adv Mater*, 2020, 32, 1907937
- [108] Zhu H F, Li J L, Chen Q, et al. Highly tunable lateral homojunction formed in two-dimensional layered CuInP<sub>2</sub>S<sub>6</sub> via in-plane ionic migration. *ACS Nano*, 2023, 17, 1239
- [109] Cai Z Y, Liu B L, Zou X L, et al. Chemical vapor deposition growth and applications of two-dimensional materials and their heterostructures. *Chem Rev*, 2018, 118, 6091
- [110] Zhu J D, Park J H, Vitale S A, et al. Low-thermal-budget synthesis of monolayer molybdenum disulfide for silicon back-end-of-line integration on a 200 mm platform. *Nat Nanotechnol*, 2023, 18, 456
- [111] Zhang K N, She Y H, Cai X B, et al. Epitaxial substitution of metal iodides for low-temperature growth of two-dimensional metal chalcogenides. *Nat Nanotechnol*, 2023, 18, 448
- [112] Li T T, Guo W, Ma L, et al. Epitaxial growth of wafer-scale molybdenum disulfide semiconductor single crystals on sapphire. *Nat Nanotechnol*, 2021, 16, 1201
- [113] Fu Q, Dai J Q, Huang X Y, et al. One-step exfoliation method for

- plasmonic activation of large-area 2D crystals. *Adv Sci*, 2022, **9**, 2204247
- [114] Huang Y, Pan Y H, Yang R, et al. Universal mechanical exfoliation of large-area 2D crystals. *Nat Commun*, 2020, **11**, 2453
- [115] Lee Y C, Chang S W, Chen S H, et al. Optical inspection of 2D materials: From mechanical exfoliation to wafer-scale growth and beyond. *Adv Sci*, 2022, **9**, 2102128
- [116] Zou Z X, Liang J W, Zhang X H, et al. Liquid-metal-assisted growth of vertical GaSe/MoS<sub>2</sub> p–n heterojunctions for sensitive self-driven photodetectors. *ACS Nano*, 2021, **15**, 10039
- [117] Zhao S W, Wu J C, Jin K, et al. Highly polarized and fast photoresponse of black phosphorus-InSe vertical p–n heterojunctions. *Adv Funct Mater*, 2018, **28**, 1802011
- [118] Liu H W, Zhu X L, Sun X X, et al. Self-powered broad-band photodetectors based on vertically stacked WSe<sub>2</sub>/Bi<sub>2</sub>Te<sub>3</sub> p–n heterojunctions. *ACS Nano*, 2019, **13**, 13573
- [119] Li S N, Zhang J L, Zhu L Y, et al. Reconfigurable and broadband polarimetric photodetector. *Adv Funct Mater*, 2023, **33**, 2210268
- [120] Wu F, Xia H, Sun H D, et al. AsP/InSe van der Waals tunneling heterojunctions with ultrahigh reverse rectification ratio and high photosensitivity. *Adv Funct Mater*, 2019, **29**, 1900314
- [121] Wu F, Li Q, Wang P, et al. High efficiency and fast van der Waals hetero-photodiodes with a unilateral depletion region. *Nat Commun*, 2019, **10**, 4663
- [122] Jin B, Zuo N, Hu Z Y, et al. Excellent excitonic photovoltaic effect in 2D CsPbBr<sub>3</sub>/CdS heterostructures. *Adv Funct Mater*, 2020, **30**, 2006166
- [123] Zeng P Y, Wang W H, Han D S, et al. MoS<sub>2</sub>/WSe<sub>2</sub> vdW heterostructures decorated with PbS quantum dots for the development of high-performance photovoltaic and broadband photodiodes. *ACS Nano*, 2022, **16**, 9329
- [124] Ma C, Shi Y M, Hu W J, et al. Heterostructured WS<sub>2</sub>/CH<sub>3</sub>NH<sub>3</sub>PbI<sub>3</sub> photoconductors with suppressed dark current and enhanced photodetectivity. *Adv Mater*, 2016, **28**, 3683
- [125] Ning W H, Wang F, Wu B, et al. Long electron-hole diffusion length in high-quality lead-free double perovskite films. *Adv Mater*, 2018, **30**, 1706246
- [126] Chen S, Shi G Q. Two-dimensional materials for halide perovskite-based optoelectronic devices. *Adv Mater*, 2017, **29**, 1605448
- [127] Fang F E, Wan Y, Li H N, et al. Two-dimensional Cs<sub>2</sub>AgBiBr<sub>6</sub>/WS<sub>2</sub> heterostructure-based photodetector with boosted detectivity via interfacial engineering. *ACS Nano*, 2022, **16**, 3985
- [128] Wang L M, Zou X M, Lin J, et al. Perovskite/black phosphorus/MoS<sub>2</sub> photogate reversed photodiodes with ultrahigh light on/off ratio and fast response. *ACS Nano*, 2019, **13**, 4804
- [129] Yang S, Cha J, Kim J C, et al. Monolithic interface contact engineering to boost optoelectronic performances of 2D semiconductor photovoltaic heterojunctions. *Nano Lett*, 2020, **20**, 2443
- [130] Lee I, Kang W T, Kim J E, et al. Photoinduced tuning of Schottky barrier height in graphene/MoS<sub>2</sub> heterojunction for ultrahigh performance short channel phototransistor. *ACS Nano*, 2020, **14**, 7574
- [131] Zhang J, Cong L, Zhang K, et al. Mixed-dimensional vertical point p–n junctions. *ACS Nano*, 2020, **14**, 3181
- [132] Wang Q H, Kalantar-Zadeh K, Kis A, et al. Electronics and optoelectronics of two-dimensional transition metal dichalcogenides. *Nat Nanotechnol*, 2012, **7**, 699
- [133] Mak K F, Shan J. Photonics and optoelectronics of 2D semiconductor transition metal dichalcogenides. *Nat Photonics*, 2016, **10**, 216
- [134] Wu D, Guo J W, Du J, et al. Highly polarization-sensitive, broadband, self-powered photodetector based on graphene/PdSe<sub>2</sub>/germanium heterojunction. *ACS Nano*, 2019, **13**, 9907
- [135] Zeng L H, Chen Q M, Zhang Z X, et al. Multilayered PdSe<sub>2</sub>/perovskite Schottky junction for fast, self-powered, polarization-sensitive, broadband photodetectors, and image sensor application. *Adv Sci*, 2019, **6**, 1901134
- [136] Zhou J D, Lin J H, Huang X W, et al. A library of atomically thin metal chalcogenides. *Nature*, 2018, **556**, 355
- [137] Xie C, Zeng L H, Zhang Z X, et al. High-performance broadband heterojunction photodetectors based on multilayered PtSe<sub>2</sub> directly grown on a Si substrate. *Nanoscale*, 2018, **10**, 15285
- [138] Wu E P, Wu D, Jia C, et al. In situ fabrication of 2D WS<sub>2</sub>/Si type-II heterojunction for self-powered broadband photodetector with response up to mid-infrared. *ACS Photonics*, 2019, **6**, 565
- [139] Xiao P, Mao J, Ding K, et al. Solution-processed 3D RGO-MoS<sub>2</sub>/pyramid Si heterojunction for ultrahigh detectivity and ultra-broadband photodetection. *Adv Mater*, 2018, **30**, 1801729
- [140] Chen W J, Liang R R, Zhang S Q, et al. Ultrahigh sensitive near-infrared photodetectors based on MoTe<sub>2</sub>/germanium heterostructure. *Nano Res*, 2020, **13**, 127
- [141] Lei W, Antoszewski J, Faraone L. Progress, challenges, and opportunities for HgCdTe infrared materials and detectors. *Appl Phys Rev*, 2015, **2**, 041303
- [142] Wang Y, Gu Y, Cui A L, et al. Fast uncooled mid-wavelength infrared photodetectors with heterostructures of van der Waals on epitaxial HgCdTe. *Adv Mater*, 2022, **34**, 2107772
- [143] Jiao H X, Wang X D, Chen Y, et al. HgCdTe/black phosphorus van der Waals heterojunction for high-performance polarization-sensitive midwave infrared photodetector. *Sci Adv*, 2022, **8**, eabn1811
- [144] Nadupalli S, Kreisel J, Granzow T. Increasing bulk photovoltaic current by strain tuning. *Sci Adv*, 2019, **5**, eaau9199
- [145] Kushnir K, Wang M J, Fitzgerald P D, et al. Ultrafast zero-bias photocurrent in GeS nanosheets: promise for photovoltaics. *ACS Energy Lett*, 2017, **2**, 1429
- [146] Ai H Q, Liu D, Geng J Z, et al. Theoretical evidence of the spin-valley coupling and valley polarization in two-dimensional MoSi<sub>2</sub>X<sub>4</sub> (X = N, P, and As). *Phys Chem Chem Phys*, 2021, **23**, 3144
- [147] Jiang J, Chen Z Z, Hu Y, et al. Flexo-photovoltaic effect in MoS<sub>2</sub>. *Nat Nanotechnol*, 2021, **16**, 894
- [148] Park N G, Segawa H. Research direction toward theoretical efficiency in perovskite solar cells. *ACS Photonics*, 2018, **5**, 2970
- [149] Rühle S. Tabulated values of the Shockley–Queisser limit for single junction solar cells. *Sol Energy*, 2016, **130**, 139
- [150] Spanier J E, Fridkin V M, Rappe A M, et al. Power conversion efficiency exceeding the Shockley–Queisser limit in a ferroelectric insulator. *Nat Photonics*, 2016, **10**, 611
- [151] Han H, Song S, Lee J H, et al. Switchable photovoltaic effects in hexagonal manganite thin films having narrow band gaps. *Chem Mater*, 2015, **27**, 7425
- [152] Bai Y, Jantunen H, Juuti J. Ferroelectric oxides for solar energy conversion, multi-source energy harvesting/sensing, and opto-ferroelectric applications. *ChemSusChem*, 2019, **12**, 2540
- [153] Zhang Y, Holder T, Ishizuka H, et al. Switchable magnetic bulk photovoltaic effect in the two-dimensional magnet CrI<sub>3</sub>. *Nat Commun*, 2019, **10**, 3783
- [154] Ding W J, Zhu J B, Wang Z, et al. Prediction of intrinsic two-dimensional ferroelectrics in In<sub>2</sub>Se<sub>3</sub> and other III<sub>2</sub>-VI<sub>3</sub> van der Waals materials. *Nat Commun*, 2017, **8**, 14956
- [155] Li Y, Fu J, Mao X Y, et al. Enhanced bulk photovoltaic effect in two-dimensional ferroelectric CuInP<sub>2</sub>S<sub>6</sub>. *Nat Commun*, 2021, **12**, 5896
- [156] Akamatsu T, Ideue T, Zhou L, et al. A van der Waals interface that creates in-plane polarization and a spontaneous photovoltaic effect. *Science*, 2021, **372**, 68
- [157] Qin F, Shi W, Ideue T, et al. Superconductivity in a chiral nanotube. *Nat Commun*, 2017, **8**, 14465
- [158] Yadgarov L, Višić B, Abir T, et al. Strong light-matter interaction in tungsten disulfide nanotubes. *Phys Chem Chem Phys*, 2018, **20**, 20812
- [159] Zhang C Y, Wang S, Yang L J, et al. High-performance photodetectors for visible and near-infrared lights based on individual WS<sub>2</sub> nanotubes. *Appl Phys Lett*, 2012, **100**, 243101

- [160] Jariwala D, Davoyan A R, Wong J, et al. Van der Waals materials for atomically-thin photovoltaics: promise and outlook. *ACS Photonics*, 2017, 4, 2962
- [161] Schmidt H, Giustiniano F, Eda G. Electronic transport properties of transition metal dichalcogenide field-effect devices: surface and interface effects. *Chem Soc Rev*, 2015, 44, 7715
- [162] Vu Q A, Yu W J. Electronics and optoelectronics based on two-dimensional materials. *J Korean Phys Soc*, 2018, 73, 1
- [163] Manzeli S, Ovchinnikov D, Pasquier D, et al. 2D transition metal dichalcogenides. *Nat Rev Mater*, 2017, 2, 17033
- [164] Lee D H, Lee J J, Kim Y S, et al. Remote modulation doping in van der Waals heterostructure transistors. *Nat Electron*, 2021, 4, 664
- [165] Li W S, Gong X S, Yu Z H, et al. Approaching the quantum limit in two-dimensional semiconductor contacts. *Nature*, 2023, 613, 274
- [166] Lemme M C, Daus A. Low-temperature MoS<sub>2</sub> growth on CMOS wafers. *Nat Nanotechnol*, 2023, 18, 446
- [167] Ma K Y, Zhang L N, Jin S, et al. Epitaxial single-crystal hexagonal boron nitride multilayers on Ni (111). *Nature*, 2022, 606, 88
- [168] Xu X L, Pan Y, Liu S, et al. Seeded 2D epitaxy of large-area single-crystal films of the van der Waals semiconductor 2H MoTe<sub>2</sub>. *Science*, 2021, 372, 195
- [169] Yuan G W, Liu W L, Huang X L, et al. Stacking transfer of wafer-scale graphene-based van der Waals superlattices. *Nat Commun*, 2023, 14, 5457
- [170] Liu G Y, Tian Z A, Yang Z Y, et al. Graphene-assisted metal transfer printing for wafer-scale integration of metal electrodes and two-dimensional materials. *Nat Electron*, 2022, 5, 275



**Haoyun Wang** received his B.S. degree in functional materials from Huazhong University of Science and Technology (HUST) in Wuhan, China in 2020. Currently, he is pursuing a doctor's degree in material physics and chemistry from HUST. His current research interest is focused on 2D materials based electronic and optoelectronic devices.



**Xingyu Song** received her B.S. degree in materials science and engineering from Northeastern University in Shenyang, China in 2021. Currently, she is pursuing a M.S. degree in materials science from Huazhong University of Science and Technology in Wuhan. Her current research interest is focused on 2D materials based tunneling transistors.



**Xing Zhou** is a Professor of School of Materials Science and Engineering, Huazhong University of Science and Technology (HUST). He received his B.S. degree in inorganic nonmetallic materials from Wuhan University of Science and Technology (WUST) in 2012, and received his Ph.D. from HUST in 2017. His current research interests focus on the controllable synthesis of 2D materials and their heterostructures for optoelectronics.



**Tianyou Zhai** received his B.S. degree in chemistry from Zhengzhou University in 2003, and then received Ph.D. degree in physical chemistry from the Institute of Chemistry, Chinese Academy of Sciences (ICCAS) in 2008. Afterward, he joined the National Institute for Materials Science (NIMS) as a JSPS postdoctoral fellow, and then as an ICYS-MANA researcher within NIMS. Currently, he is a Chief Professor of School of Materials Science and Engineering, Huazhong University of Science and Technology (HUST). His research interests include the controlled synthesis and exploration of fundamental physical properties of inorganic functional nanomaterials, as well as their applications in optoelectronics.